IISc Theses Abstracts

Contents

J. Indian Inst. Sci., July–Aug. 1993, 73, 367–427
© Indian Institute of Science

IISc THESES ABSTRACTS

Thesis Abstract (M.Sc.(Engng))

Fault diagnosis and diagnosability in multiprocessor systems by G. Elango
Research supervisor: Lawrence Jenkins
Department: Electrical Engineering

1. Introduction

In multiprocessor systems, fault tolerance is achieved by the identification of faulty processors, and the subsequent reconfiguration and recovery of the system. In such systems, each processor is required to periodically test some of the other processors with which it is connected. When a healthy processor tests a faulty one, it indicates the presence of a fault; at other times, it indicates that the system is healthy. The test results are represented by a directed graph, in which the nodes represent the processors, and the edges represent the tests. An edge (i, j) has the label 0 if the ith processor evaluates the jth processor as healthy, and 1 if it evaluates it as faulty. Since the tests that are carried out by a faulty processor are invalid a 1 link indicates that either or both of the processors at its ends must be faulty. The collection of test results is a syndrome; fault diagnosis is the process of associating a set of faulty processors with a specified syndrome.

2. Main results and conclusions

In this work, algorithms have been developed for the diagnosis of systems which have special interconnection patterns. The system structure has been exploited to obtain improved performance, as compared with existing algorithms[1].

The main thrust of the work is diagnosability of hybrid fault situations. In diagnosability characterization, it has often been assumed that all faults are permanent, and that they do not propagate[2]. This is not always realistic, since some faults are intermittent, and are manifest only some of the time; when intermittently fault processors are permitted, the situation is referred to as the hybrid fault situation. Faults can propagate, because when a faulty processor interacts with a healthy processor, the healthy processor can become either intermittently or permanently faulty. The diagnosis of the hybrid fault situation is inherently difficult, because the fault may be manifest, producing a 1 result, when some healthy processor tests it, and it may not be manifest when another processor tests it. This work extends diagnosis results to hybrid fault situations in which fault propagation is allowed.

Three new diagnosability measures have been defined; all of these refer to hybrid faults[3], with fault propagation. It is shown that these measures encompass as a special case the earlier measure which refers to the permanent fault situation with no propagation. Characterizations for all the corresponding diagnosabilities are given, and the most general one is analysed in depth. The relationships among the three diagnosabilities are established, and the interrelationships between their parameters obtained.

Diagnosability results have been obtained for the asymmetric invalidation model[4] in which it is assumed that whenever a permanently faulty processor tests another permanently faulty processor, it will always indicate the presence of a fault. A new diagnosability measure has been obtained for the hybrid fault situation with the asymmetric invalidation model, in the presence of fault propagation. The corresponding diagnosability has been characterized for this measure.

Graph theory has been applied to the disagreement graphs that correspond to the permanent fault

situation with fault propagation. It has been established that the vertex cover set[5] of the disagreement graph is a subset of the fault set and accounts for the syndrome. This result is of significance to the development of an efficient fault diagnosis algorithm.

References

1.	DAHBURA, A T. AND MASSON, G M	An $O(n^{2.5})$ fault identification algorithm for diagnosable systems, *IEEE Trans* , 1984, **C–33**, 486–492
2	CHUA, K T. AND HAKIMI, S.L.	On fault identification in diagnosable systems, *IEEE Trans.*, 1981, C-30. 414–422
3.	DAHBURA, A T. AND MASSON, G M.	Greedy diagnosis of hybrid fault situations, *IEEE Trans.*, 1983, C-32. 777–782.
4.	HUANG, K.	Diagnosability of system faults with propagation under asymmetric invalidation, *Microprocessing Microprog.*, 1988, 723–730.
5.	BONDY, J.A. AND MURTHY, V.S.R	*Graph theory with applications*, 1976, Elsevier–North-Holland.

Thesis Abstract (Ph.D.)

A study of an R&D team in an Indian research organization: An ethnographic approach by V. Suchitra Mouly

Research supervisors: Esther Ramani and A.K.N. Reddy
Department: Management Studies

1. Introduction

This research aims to provide a descriptive–analytical case study of an R&D team in a government-sponsored and funded organization in southern India. It aims to understand the microculture that is assumed to underlie both the generation and interpretation of communicative behaviour among the members of this R&D team. We provide an information base grounded in insiders' perceptions of their daily life at work and hope to facilitate an understanding of both the strengths and weaknesses of Indian R&D life.

This research is an alternative to two different but deep-rooted trends in the study of scientific organizations in India. By and large, over the last fifty years, sociological studies of S&T in India have focussed on macro-level aspects such as institution building, policy making, planning and implementation of programmes. Indepth studies of the functioning of specific research teams in S&T institutions are not available. Micro-level descriptions focussing on the interactions between members of an R&D team and the patterns of communication between them are still lacking in the Indian context. Where studies of specific organizations have been undertaken, the focus has been on testing hypotheses and establishing relationships among different variables. Often, based on surveys, these studies have been within a quantitative paradigm, and do not emphasize insiders' perceptions. Our research therefore attempts to provide a micro-level qualitative study as opposed to both macro-level sociological studies of S&T and organization-based quantitative studies in India.

2. Objectives and methodology

The objective of this study is to provide a 'thick description' of Indian R&D life by consolidating the members' experience of their R&D projects[1]. We try to understand, through this research, the nature and structure of one Indian R&D team, the kinds of interactions that occur, the importance of organizational structure, whether it facilitates or impedes communication, and its relation to productivity and performance.

As an alternative to the quantitative survey research mode which dominates organizational studies in the Indian context, this research explores an ethnographic form of inquiry. In fact, the central concern of this work is to argue for a more qualitative approach to the study of R&D life in India, and to demonstrate the conceptual coherence and methodological viability of such an approach.

Ethnography, which is a descriptive study of a given culture, originates in cultural anthropology. It aims to describe the nature of interactions that occur among the members of a community on a day-to-day basis. The emphasis in ethnography is on understanding another way of life, and not on seeking objectively valid generalizations[2,3]. We use ethnographic research tools for our fieldwork, *viz.*, participant observation and ethnographic interviews[4]. We also developed a communication study questionnaire for this study.

3. Major findings and conclusions

Our research suggests that R&D cultures may be heterogeneous (as opposed to the prevalent view that organizations are homogeneous) and could be made up of different subcultures. It also suggests that it may be productive to view an Indian R&D organization as simultaneously belonging to a larger primary culture, while itself comprising several subcultures. The presence of these competing subcultures may be seen in the conflicting images of selfhood that members of an R&D organization hold.

The research challenges a dominant view in organization studies that superior–subordinate relationships are fixed and thus constitute the crux of organizational behaviour. Our research reveals that R&D members seem to simultaneously experience both superior and subordinate roles in different organizational groupings, and their self-images, which crucially affect their organizational behaviour, are based on shifting perceptions of their power to affect decision-making in specific groupings.

Notions such as 'success' and 'failure' in R&D projects cannot be 'objectively' defined. Our study suggests that members' experiences shape their definitions. Further, members at different levels in the R&D hierarchy define success/failure in divergent ways. Where there is little convergence between these perceptions, a sense of personal apathy and frustration may prevail.

The view that is prevalent in the management science literature that organizations have cultures is challenged by this study which is based on the notion that organizations are cultures. Further, these cultures are complex derivatives of a primary culture and several professional subcultures.

Finally, this research challenges the dominant mode of investigation in Indian organizational settings, the survey research mode, and offers a viable alternative to it, the ethnographic research mode[6]. Our methodological finding is that even a partial suggestive ethnography gives us insights into the particular ways in which members of a culture make sense of the universe they inhabit.

Apart from these specific, substantive findings, this research also discusses methodological findings such as the role of subjectivity in qualitative research, the ethical dimensions of ethnographic research, and the issue of generalizability of the research findings.

References

1. GEERTZ, C. — *Local knowledge*, 1973, Basic Books, New York.
2. AGAR, M. — *The professional stranger. An informal introduction to ethnography*, 1980, Academic Press.
3. ATKINSON, P. AND HAMMERSLEY, M. — *Ethnography: Principles in practice*, 1983, Tavistock, London.
4. SPRADLEY, J.P. — *The ethnographic interview*, 1979, Holt, Rinehart and Winston.
5. SPRADLEY, J.P. — *Participant observation*, 1980, Holt, Rinehart and Winston.
6. MOULY, V. S. AND RAMANI, E. — Survey research and ethnographic research: An appraisal of two research methodologies, *Mgmt Rev.*, 1990, **5**, 31–51.

Thesis Abstract (Ph.D.)

Studies of the vibrational and magnetic properties of the layered compounds b
Radhika Rani Rao
Research supervisor: A.K. Raychaudhuri
Department: Physics

1. Introduction

Among the large family of layered materials[1], transition metal phosphorus trisulfides represented by MPS_3 (where M is a transition element, P, phosphorus, and S, sulphur) form a class by themselves with interesting structural and magnetic properties[2]. The anisotropy in the physical properties gives rise to a host of interesting features in these two-dimensional compounds These compounds are isostructural having $CdCl_2$-type structure with monoclinic symmetry and space group $C2/m$[3,4].

In the present investigation, we have studied the structural, vibrational and magentic properties of $FePS_3$, $NiPS_3$ and their solid solutions $Fe_{1-x}Ni_x$ PS_3 ($0 \leq \times \leq 1$). We have found that in the solid solutions, the replacement of Fe by Ni causes change in the relative strengths of inter and intralayer couplings leading to a change in the anisotropy. In this sense it may be said that we can 'tune' the anisotropy by chemical compositional changes. Our objective in this work is to look at the tuning of anisotropy as one goes from $FePS_3$ to $NiPS_3$ and how it reflects in the vibrational and magnetic properties.

2. Experimental work

All the compounds were prepared by the method of Klingen *et al* [5]. X-ray diffraction studies were carried out on a Philips diffractometer (Model PW 1050) using Co-K_α radiation. The IR spectra were recorded using IR Bruker IFS 113-V FTIR spectrometer Magnetic susceptibility was measured by Faraday balance method using Cahn 1000RG electrobalance. The vibrating sample magnetometer (EG&G Par Model 155) was used to measure field- and zero field-cooled susceptibilities.

3. Results and discussion

From the structural analysis, we show that there is a lattice compaction as the composition x is varied from 0 to 1, maintaining the same basic lattice symmetry. We find that the relative compaction is more in the basal plane. These subtle structural changes are reflected in the vibrational spectrum and they also determine the spin state of the ions We have found that most dominant change in the structure comes from d_{M-s} (M–S distance) and the lattice contracts on going from $FePS_3$ to $NiPS_3$. From the infrared (IR) spectroscopic studies on the solid solutions, $Fe_{1-x}Ni_xPS_2$ at room temperature, we point out that there are interesting changes in the vibrational spectra when Ni is substituted for Fe. The high-frequency ($\omega > 300$ cm^{-1}) modes arise from the $(P_2S_6)^{4-}$ unit and they do not get affected much by cation substitution but the low-frequency ($\omega < 300$ cm^{-1}) bands are sensitive to cation substitution. There are significant changes in the vibrational modes (including splitting of the bands) which may arise from $FePS_3$ to $NiPS_3$. The low-frequency split bands (in the range 150–200 cm^{-1}) and the doublets around (280–302 cm^{-1}) region are the new features of our data. We have tried to explain the splitting of the bands as arising from correlation splitting and the doublet arises due to reduction in the interlayer coupling. From the temperature dependence of IR spectra of $FePS_3$ we have found an interesting point that some of the changes brought about by the contraction of the lattice in going from $FePS_3$ to $NiPS_3$ can also be brought about by cooling $FePS_3$. This also happens due to preferential compaction in the layer.

The fact that $FePS_3$ and $NiPS_3$ are both antiferromagnets at low temperatures with different types of magnetic interaction gives rise to the interest in the mixed antiferromagnetic systems. $FePS_3$ is essentially an Ising system with strong anisotropy and $NiPS_3$ is an Heisenberg system with weak anisotropy[5]. This essential difference comes from the crystal fields and the difference in the ground state term of these two ions Fe^{2+} and Ni^{2+} (Fe^{2+} – d^6, Ni^{2+} – d^8). In the present work, we have investigated the interesting effects of substituting Ni^{2+} (with weak anisotropy) in the essentially Ising system $FePS_3$ (with strong anisotropy). All the compounds show a maximum in χ at a temperature T_{max} followed by the onset of antiferromagnetic order at low temperatures at T_N. As the composition is changed there is a continuous change in T_N and also in the ratio T_N/T_{max}. Our results show that in the mixed antiferromagnetic system $Fe_{1-x}Ni_xPS_3$ the strongly anisotropic Fe component imposes its anisotropy on weakly anisotropic Ni component. We find also no frustration or spin glass-like ordering at any composition.

We have also presented Mossbauer spectroscopy results on $Fe_{1-x}NiPS_2$ ($0 \leq \times \leq 0{\cdot}8$). We have calculated the composition and also tried to estimate the effective valence of Fe^{2+} for the mixed systems.

References

1. LEITH, R M.A — *Physics and chemistry of materials with layered structure*, Vol. 1, 1977, D. Reidel.
2. BREC, R — *Solid St. Ionics*, 1986, 22, 3–30.
3. KLINGEN, V.W., EULENBERGER, G AND HAHN, H. — *Z. Anorg Alleg Chem.*, 1973, **401**, 97–112
4. OUVRARD, G., BREC, R. AND HAHN, H. — *Mat Res Bull.*, 1985, **20**, 1181–1189
5. KLINGEN, V.W , OTT, R AND HAHN, H. — *Z. Anorg Alleg. Chem.*, 1973, **396**, 271–278.
6. JOY, P.A. — *Layered transition metal theophosphates: A study of their properties and intercalation chemistry*, Ph.D. Thesis, Indian Institute of Science, Bangalore, 1990.

Thesis Abstract (Ph.D.)

Investigations of reentrant phase transitions in quasi-binary liquid mixtures by T. Narayanan
Research supervisors: E.S.R. Gopal and Anil Kumar
Department: Physics

1. Introduction

The reentrant phase transitions (RPT) imply that a system reenters a state macroscopically identical to the initial one, after two or more phase transitions, when a convenient thermodynamic field variable is altered monotonically[1]. Quasi-binary liquid mixtures are prime examples of the systems which manifest this phenomena[1-5]. A typical reentrant binary liquid mixture exhibits a closed-loop phase diagram whose maximum and minimum define the upper and lower critical solution temperatures (T_U and T_L, respectively); its loop size (ΔT) = $T_U - T_L$. A double critical point (DCP) is realized when $\Delta T \approx 0$.

The 3D Ising-like critical behaviour near a T_U or T_L (when they are far apart) is well understood[6]. Thus, it is interesting to examine the nature of DCP as it is formed by the coalescence of a T_U and T_L coupled with the fact that the locus of T_Us and T_Ls is parabolic in nature in the appropriate field space[1-5]. In a binary liquid mixture with closed-loop miscibility curve, ΔT can be controlled with the aid of a suitable third component[1-5,7].

The theoretical models[8] concerning RPT in quasi-binary liquid mixtures predict a doubling of critical exponents (CE) in the close vicinity of DCP. However, experimental investigations prior to this work[2-4] could not yield an exact doubling of CEs due to the fact that the DCP was not probed close enough. Furthermore, the question regarding the nature of doubled CEs (Ising or mean field) also remained unanswered[4].

The present investigation is aimed (i) to observe the exact doubling of CEs by proving a ΔT as small as feasible and hence to reveal the true nature of doubled CEs, (ii) to describe the critical behaviour for any ΔT by the same universal CE using a suitable alternate field variable.

The quasi-binary system studied are: 3-methylpyridine (MP)+water (W)+heavy water (HW) and MP+W+NaCl. The quantities measured are electrical resistance (R) and phase diagram (order parameter).

2. Experimental

The quasi-binary mixtures were made using MP (99%, Aldrich), HW (isotopic purity 99·6%, BARC, India), freshly prepared W in an all-quartz triple distiller and analytical-grade NaCl (Ranbaxy, India). The

chemicals were transferred with air-tight syringes (Hamilton) and weighed in an analytical balance with resolution of 10μg. The conductivity cells with perforated circular platinum electrodes were blown fro Pyrex glass tubes. The sample cells used for the visual observation of phase diagram were also made o of Pyrex glass with typical volume of 2 ml.

The indispensible instrumentation fabricated for the present study are: (a) 2-stage paraffin oil thermos with millidegree temperature controller (PID), (b) ac impedance bridge (ratio transformer based) with resolution of 10 ppm The temperature was measured using a calibrated (IPTS-68) PRT in conjuncti with an ac bridge (ASL, UK) up to a resolution of 0·26 mK. The detector used in the impedance brid was a lock-in amplifier (SRS, USA). The R measurements were performed at spot frequencies 10, 20, and 40 kHz. Lower frequencies were not probed due to possible significant contribution from electro polarization and higher frequencies have instrument systematic errors. A typical run scanned the ran $0{\cdot}001 \leq |T_C - T| \leq 5°C$, where T_C is T_U or T_L and spanned 48–72 h. The measurements encompassed t ΔTs; $78°C \leq \Delta T \leq 1{\cdot}01°C$, near T_L for MP+W+WH, $30{\cdot}96°C \leq \Delta T \leq 1{\cdot}67°C$, near T_L and 21°C $\Delta T \leq 1{\cdot}9°C$, near T_U for MP+W+NaCl.

The major experimental difficulties encountered are the temporal instability in R and ΔT and obtaini the correct critical concentration (x_c) for each sample[1-7]. In this regard, MP+W+NaCl is a better syst compared to MP+W+HW, as the former yields a swift equilibration in R and ΔT. Furthermore, t quantity of salt needed is very small (<0·2% by weight) and hence the binary nature of the system preserved. The closed-loop phase diagram ($\Delta T = 22{\cdot}06°C$) of MP+W+HW was determined visually. T system was preferred to salt-doped MP+W because of the better control in obtaining a given ΔT.

3. Results

The following expression adequately describes the measured R data for MP+W+HW

$$R = R_C + A_1 t + A_2 t^2 + A_3 t^{\theta} + A_4 t^{\theta+\Delta}, \qquad (1$$

where R_C is R as $t \to 0$; $t = |(T_C - T)/T_C|$; A_1–A_4, the fitting parameters, θ, the CE and Δ, t correction-to-scaling exponent[6] (= 0·5). A nonlinear least squares fit to eqn 1 was performed using t program CURFIT[9]. The retention of A_4 term did not improve the fit significantly and it was discard The results of the three-parameter (A_1–A_3) fit indicated an effective increase in the value of θ from possible theoretical estimate[1] (=2β) to a doubled limit (within 7%) as ΔT was reduced from 78°C 1·01°C. Figure 1 depicts the variation of effective θ with ΔT. The results supported an exact doubling CEs in terms of their Ising values in the limit of DCP[1].

The analysis of R data for the system MP+W+NaCl using eqn 1 showed some discrepancies in results near T_U to those near T_L, which are otherwise expected to be the same. This led us to reconsi the validity of the field variable t to describe the critical behaviour in RPT. An alternate way of describ RPT is to consider the simultaneous access to both T_U and T_L[5,7]. This can be accomplished very con niently using the field variable $t_{UL} = |[T_U - T)(T_L - T)]/T_U T_L|$. The choice of this field variable follc from the geometrical picture of phase transitions as well as Landau–Ginzburg theory of RPT[5,7]. Furth more, the use of t_{UL} recovers the universal value of θ for any ΔT. The following expresssion was sufficie to describe the R data both near T_U and T_L.

$$R = R_C + R_1 t + R_2 t_{UL}^{0.65} + R_3 t_{UL}^{0.89} \qquad (2$$

where R_1–R_3 are the fitting parameters. Terms involving two possible analytical estimates for θ (2β ≈ 1–α) were found to be essential for conserving the uniformity near T_U and T_L. The doubling of the C in the vicinity of DCP can be visualized[7] from the expanded form of t_{UL} [$= t^2 + (\Delta T/T_C)\, t$]. At DC $\Delta T = 0$, $t_{UL} = t^2$ and hence the doubling of *CEs*, if the field variable employed is t. For very large Δ the term dominates and Ising-like critical behaviour persists. For intermediate ΔTs, the situation is sor what complex as a result of the competition between t^2 and t terms. Far away from T_C, t^2 term leads o t term and *vice versa* near T_C. Thus, the phenomenon becomes a crossover[7] from the doubled CE to single CE limit as t is decreased to 0.

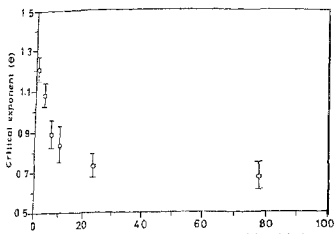

FIG. 1. Variation of the critical exponent (θ) with loop size Here θ represent an *effective* critical exponent.

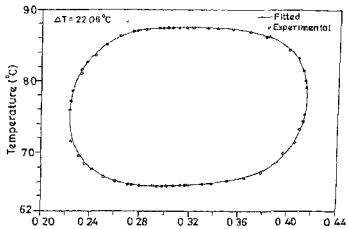

FIG 2. The closed-loop phase diagram of the quasi-binary liquid mixture MP+W+HW with a loop size of 22.06° C. The solid line is generated by the best fit parameters to eqn. 3.

The validity of t_{UL} for the analysis of RPT was further supplemented as the following expressions completely described the closed-loop phase diagram and its diameter, respectively,

$$x^{+} - x^{-} = B\, t_{UL}^{\beta} \tag{3}$$

$$\frac{x^{+}+x^{-}}{2} = x_C + D_1 t + D_2 t_{UL}^{0.65} + D_3 t_{UL}^{0.89} \tag{4}$$

where B and D_1–D_3 are fitting parameters. The striking feature of this method of analysis is that the entire closed-loop phase diagram (shown in Fig. 2) is adequately fitted with eqn 3. Moreover, the fit preserved the Ising value of β (0·325) to within 2%. Similarly, the diameter of the closed-loop phase diagram pertains to an identical function[6] (eqn 4) as that of normal binary mixtures.

4. Discussion

Our findings confirm that near a DCP a doubling of 3D-Ising CEs occurs in consonance with the geometrical picture of phase transitions and model calculations. Invoking a new field variable (t_{UL}) enabled us to characterize any experimental path of approach (involving variation of temperature) to the reentrant critical line (including the DCP) by the same universal CE, which refers to a normal single critical point for any given property. This idea has been successfully tested for two different properties: the electrical resistance and the order parameter.

References

1. NARAYANAN, T., KUMAR, A. AND GOPAL, E.S.R. *Phys. Lett. A*, 1990, **144**, 371-375.
2. JOHNSTON, R.G , CLARK, N.A., WELTZIUS, P. AND CANNELL, D.S. *Phys. Rev. Lett.*, 1985, **54**, 49–52.
3. SORENSEN, C.M. AND LARSEN, G.A. *J. Chem. Phys.*, 1985, **83**, 1835–1842.
4. ZAITSEV, V.P., KRIVOKHIZHA, S.V., FABELINSKII, I.L., TSITROVSKII, A., CHAIKOV, L.L., SHVETS, E.V. AND YANI, P. *Sov. Phys. JETP Lett.*, 1986, **43**, 112–116.
5. DAVIDOVICH, L.A. AND SHINDER, I.I. *Sov. Phys. JETP*, 1989, **68**, 743–750.
6. KUMAR, A., KRISHNAMURTHY, H.R. AND GOPAL, E.S.R. *Phys. Rep.*, 1983, **98**, 57–143.
7. NARAYANAN, T., KUMAR, A. AND GOPAL, E.S.R. *Phys. Lett. A.*, 1991, **155**, 276–280.
8. GOLDSTEIN, R.E. AND WALKER, J.S. *J. Chem. Phys.*, 1983, **78**, 1492–1512.
9. BEVINGTON, P.R. *Data reduction and error analysis for physical sciences*, 1969, McGraw-Hill.

Thesis Abstract (Ph.D.)

Thermodynamic properties of long chain esters: their liquid state and plasticizing havior by H.K. Shobha
Research supervisor: K. Kishore
Department: Inorganic and Physical Chemistry

1. Introduction

The liquid state behavior of long chain molecules has an important relevance in polymer chemistry. I chain esters and hydrocarbons, etc. (molecular weight 300–2000) are commonly used as plasticizer polymers[1]. A systematic study of the macroscopic liquid state properties of these long-chain liquic called for better understanding of the commonly observed deterrent phenomena of migration and vol loss of plasticizers and hence in predicting their efficiency. Despite the significance of long-chain liq in understanding the liquid state behavior in totality and their technological importance as plasticizers lubricants, it is surprising that no effort has been made hitherto to study their liquid state behavior.

In the present investigation, an attempt has been made to understand the influence of structure molecular weight of long-chain esters (molecular weight 300–900) on their macroscopic thermodyn properties such as heat of vaporization, flow and the glass transition behavior. In order to achieve above objectives, following homologous series of esters of varying molecular weight and structure l been chosen: (i) 1,10-decanediol diesters and sebacic acid diesters which are linear, flexible molecules, triglycerides and trimethylolethane triesters which are *Y* branched, compact molecules, and (iii) pentae hritol tetra esters which are + branched, rigid and highly compact molecules.

2. Results and discussion

2.1 *The flow behavior*

The absolute viscosity (η) and density data measured at different temperatures were used to obtain Δ $\Delta H^{\ddagger}$ and $\Delta S^{\ddagger}$. The plot of $\Delta H^{\ddagger}$ against molecular weight gives information about the flowing segn which corresponds to a molecular weight of about 600 for these esters[2]. The notion of blob has t invoked to describe the segmental mobility[3]. The blob size is found to decrease with branching. Th branched esters being more compact and spherical are closely packed compared to the other ester se which is consistent with the density data. The density values are more for branched esters compare linear esters[3,4-6]. In the case of $\Delta S^{\ddagger}$, their large negative values were attributed to the higher order requ in the molecules surrounding the hole for the segmental flow to occur and to the hindrance offere the branched segment in the flow process[3].

The dependence of viscosity on temperature in all the ester series was found to be non-Arrheniu the temperature range considered but the modified free volume equation, namely, Vogel, Tamm Fulcher (VTF) equation, which was used to study the temperature dependence of viscosity explains dependence of temperature in the entire temperature region. This VTF equation has also been use derive glass-transition temperature (T_g) and 'configuration entropies' (S_c) in conjunction with Adam-G equation. S_c is found to vary significantly with branching — it is the lowest in the + branched esters the highest in the linear esters. From the Angell's classification[7] of 'strong' and 'fragile' liquids, it been found that all these esters are 'fragile' liquids since they exhibit non-Arrhenius viscosity behav Besides, the molecular weight dependence of viscosity also indicates their 'fragility'[8].

3. The mechanism of vaporization

Group additivity method[9] has been used to evaluate the heat of vaporization. The calculated values w well within 5% error with the experimental values[2]. The analysis of heat of vaporization data of tl esters reveals that it is independent of molecular structure but dependent on (molecular weight)$^{2/3}$. suggests that the molecules coil up and evaporate in the form of spheres. The coiled spherical form acquired due to the intramolecular van der Waal's forces.

Succinctly, we can say that the heat of vaporization is independent of the molecular structure due to the molecules acquiring a coiled spherical form during vaporization, the heat of vaporization solely depending on the molecular weight of the esters. The flow behavior, on the other hand, seems to be dependent on structure as well as on molecular weight. Below a molecular weight of 600, the molecules flow as a whole but above it, the segmental motion ensues and the flow becomes basically independent of molecular weight.

4. The role of esters as plasticizers for PVC

The above long-chain liquid esters were used as plasticizers in PVC to assess their plasticizing behavior. The T_g of the plasticized PVC was experimentally measured by DSC and the reduction in T_g was quantified as a measure of their plasticizing ability. Structural effects on the T_g of the neat esters is well reflected in the plasticizing system. The plasticizing behavior has been explained by the PVC–plasticizer interaction using different techniques like dilute solution viscosity measurement, inverse gas chromatographic studies and from the solubility parameters by proper selection of low-molecular weight model esters[10,11]. The results were concordant with that observed in long-chain esters both as a function of molecular weight and branching.

References

1. Sears, J.K. and Touchette, N.W.	Plasticizers, In *Encyclopedia of chemical technology*, 3rd edn, (Kirk, R. and Othmer, D., eds), Vol. 18, p 111, 1982, Wiley
2. Kishore, K., Shobha, H.K. and Mattamal, G J.	*J. Phys Chem.*, 1990, **94**, 1642–1648
3. Kishore, K. and Shobha, H.K.	*J. Phys. Chem.*, 1992, **96**, 8161–8168.
4. Kishore, K. and Mattamal, G.J.	*J. Polym. Sci. Polym. Lett. Edn*, 1986, **24**, 53–55
5. Phillips, J.C. and Mattamal, G.J.	*J. Chem. Engng Data*, 1978, **23**, 1–6.
6. Shobha, H.K. and Kishore, K	*J. Chem Engng Data*, 1992, **37**, 371–376.
7. Angell, C.A.	*Chem. Rev.*, 1990, **90**, 523–542.
8. Shlesinger, M.F.	*A. Rev. Phys Chem.*, 1988, **39**, 269–290.
9. Benson, S.W	*Thermochemical kinetics*, 2nd edn, 1976, Wiley
10. Shobha, H.K. and Kishore, K.	*Macromolecules*, 1992, **25**, 6765–6769.
11. Kishore, K. and Shobha, H.K	*Indian J. Chem. A.*, 1992, **32**, 590–595.

Thesis Abstract (Ph.D.)

Spectroscopic studies on polymeric charge-transfer complexes: Poly (vinyl pyridine) donors with low molecular weight acceptors by S. Palaniappan
Research supervisor: D.N. Sathyanarayana
Department: Inorganic and Physical Chemistry

1. Introduction

Polymers are usually made electrically conducting by forming charge-transfer complexes with either electron donors or electron acceptors and the conducting property may range from an insulator to a metallic material[1-4]. Recently, extensive research on polymeric materials that are dopable to give substances that have an electrical conductivity approaching that of a metal has kindled new interest in their potential commercial applications. However, very few commercial applications of polymeric charge-transfer complexes exist today. In this context, the use of poly-(N-vinyl carbazole)-2,4,7-trinitrofluorenone, (PVK–TNF), in electrophotography[5] and of poly (2-vinyl pyridine)-iodine, (2PVP-I_2) as a cell electrode in implantable cardiac pacemakers[6] may be cited. The success of the PVK–TNF complex in the electrographic industry

organic systems can compete favourably with inorganic materials. Provided that the mechanical and processing properties can be achieved, there will probably be further applications of polymeric charge-transfer complexes.

In an effort to understand the mode, site and nature of the interaction, spectroscopic studies (UV-visible, electron paramagnetic resonance, nuclear magnetic resonance and infrared) on polymer donors, namely, poly(2-vinyl pyridine) (2PVP), poly(2-vinylpyridine-co-styrene) (2PVP-co-St), poly(4-vinyl pyridine) (4PVP) and poly(*p*-phenylene sulfide) (PPS) with iodine, *p*-chloranil (pCHL), o-chloranil (oCHL), tetracyanoethylene (TCNE), 2, 3-dichloro-5,6-dicyano-1, 4-benzoquinone (DDQ), 7,7',8,8'-tetracyanoquinodimethane (TCNQ), 2,4,7-trinitro-9-fluorenone (TNF), 2,4,5,7-tetranitro-9-fluorenone (TENF) acceptors have been carried out. For comparison with the polymeric complexes, analogous low molecular weight donors, namely, 2-picoline (2PIC) and 4-picoline (4PIC) with the same set of acceptors have also been investigated.

2. Experimental

Charge-transfer complexes have been prepared by different methods (solution, powder and melt-quench methods) and characterized by spectroscopic techniques. Absorption spectra were measured in dichloroethane at 25°C using Hitachi U-3400 spectrophotometer The EPR spectra of the complexes were obtained on a Varian E-109 spectrometer operating in the X-band. The ^{1}H NMR spectra of the complexes were recorded on a Bruker WH 270 MHz and also Varian T-60 NMR spectrometer using DMSO-d_6 as a solvent and TMS as an internal standard. IR spectra of the complexes were recorded as neat films between two KBr plates on a Perkin–Elmer 597 infrared spectrophotometer.

3. Results and discussion

Equilibrium constant (K), molar absorptivities (E), molar ratio (n), rate of forward (k_1) and backward reactions (k_{-1}) have been calculated for the charge-transfer complexes of all the polymenc as well as low molecular weight donors with the acceptors DDQ, TCNQ and I_2. The equilibrium constant and molar absorptivities for the polymeric charge-transfer complexes are much higher than those found for the corresponding model complexes, while the time required for the formation of the product from polymeric charge-transfer complexes is lower than that for the low molecular weight complexes which takes several days to form the product, and hence the product analyses are difficult. Polymer effect was observed in the vinyl pyridine polymers with large pendant n electron system. In the case of charge-transfer complexes of all the donors with pCHL and oCHL, a broad band was observed due to charge-transfer complex formation which vanishes quickly. The reaction of a donor with TCNE immediately results in a product. The complexes formed between each of the donors with TNF or TENF as an acceptor are very weak It was not possible to calculate the kinetic parameters for the complexes with pCHL, oCHL, TCNE, TNF and TENF. A new method has been proposed to determine the kinetic parameters (K, k_1, k_{-1}, E and molar ratio). This method is applicable to systems when the optical absorption is due to the charge-transfer complex and when one of the components is in large excess. This method has several advantages, for example, molar absorptivities of the polymers are not necessary, absorption need not be extrapolated to zero time of mixing, etc.

Electron paramagnetic resonance studies (both in solid and solution) are performed on the systems mentioned above. EPR signal was observed for the charge-transfer complexes of all the donors with the pCHL, oCHL, TCNQ and DDQ, whereas with I_2 and TCNE, these systems were EPR silent. Hyperfine splitting was not observed. The shape of the EPR signal is similar for the complexes of an acceptor with different polymer donors. The g-values of the complexes investigated are close to free electron g-value. The g-values and linewidths for a particular complex are independent of temperature, method of preparation and the amount of dopant used. The spin concentration of the paramagnetic charge-transfer complexes generally increases with the strength of the donor–acceptor tendencies. The paramagnetic charge-transfer complexes exhibit an exponential temperature dependence of spin concentration characteristic of semiconductors. The initially formed paramagnetic charge-transfer complexes transform finally to a diamagnetic product. However, the reaction in the solid state is extremely slow relative to that in solution.

Infrared and nuclear magnetic resonance spectra of the polymeric as well as low molecular weight complexes are examined and compared with the spectra of the components. The infrared spectra of the

complexes of all the donors with the acceptors pCHL, oCHL, DDQ, TCNQ, TCNE and I_2 show some marked changes in the band positions. For example, the C=C and C=N stretching band (usually a doublet) of picolines is shifted to higher wavenumber and the corresponding shift was not observed in the polymeric complexes. Also the absorption due to C=N stretching of the acceptor has been observed (in all the complexes) as an intense band (when the acceptors are DDQ, TCNQ and TCNE). The shifts in frequency and some alteration of intensities in the infrared spectra reflect the formation of radical ion salts.

In the ^1H NMR spectra of the complexes of 2PIC and 4PIC donors with the acceptors I_2, pCHL, oCHL, TCNQ, TCNE and DDQ, all the aromatic and methyl proton signals of picolines are shifted downfield. A possible explanation of these shifts involves induced polarization of the picoline molecule resulting from strong electrostatic interactions at the non-bonded electron pair of nitrogen. Such a polarization would lead to a more positive character at the protons and subsequent downfield shifts. The infrared and ^1H NMR spectra of the complexes of the polymeric as well as low molecular weight donors with TNF and TENF are very similar to a superposition of the spectra of their components. This is because of the lower concentration of the complexed pyridine units in the polymer chain compared to the uncomplexed one. The acceptor and donor molecules are most probably in parallel configuration.

Generally, a similar spectral behaviour was observed for each of the donors (polymeric as well as low molecular weight) with a common acceptor. The reaction of each of the donors with the acceptors pCHL, oCHL, DDQ and TCNQ showed a rapid charge-transfer complex formation which occurs with the formation of free radicals, followed by a slow reaction to a diamagnetic product. Whereas with iodine as acceptor, the rapid formation of charge-transfer complex formation, which occurs without the formation of free radicals, is followed by a slow reaction to form a product. A product is formed immediately for the reaction of a donor with TCNE as acceptor. The complex formed from the reaction of each of the donors with TNF and TENF as acceptors is weak.

References

1. FOSTER, R. (ed.) — *Molecular association*, Vol. II, pp. 80–163, 1979, Academic Press.
2. PEREDEREEVA, S.I. ORIOV, I.G. AND CHERKASHIN, M.I. — *Russ. Chem. Rev.*, 1975, **44**, 295–305.
3. GANG, E.T., NEOH, K.G. KHOR, S.H., TAN, K.K. AND TAN, B.T.G. — *Polymer*, 1990, **31**, 202–207.
4. SHIRAKAWA, H. AND IKEDA, S. — *J. Polym. Sci. Chem.*, 1974, **12**, 929–937.
5. SHAFFERT, R.M — *IBM J. Res. Dev*, 1979, **15**, 75.
6. SCHNEIDER, A.A., GREATBATCH, W. AND MEAD, R. — Power Sources 5, D H. Collins (ed.), *Proc. 9th Power Sources Symp.*, Brighton, UK, 1974, Academic Press, London, 1975.

Thesis Abstract (Ph.D.)

Numerical study of laminar mixed convection from a horizontal isothermal cylinder

by M.S. Phanikumar
Research supervisor: J. Srinivasan
Department: Mechanical Engineering

1. Introduction

Laminar flow past a horizontal circular cylinder is an important problem in fluid mechanics and it continues to be of importance due to the academic interest associated with it and its industrial importance[1]. In technology, there are several situations where an accurate estimation of heat transfer requires that the

requires that the effects of buoyancy be properly accounted for mixed convection from a cylinder is of importance in the fields of hot-wire and hot-film anemometry, heat-exchanger design, cooling of electronic equipment, design of electric transmission cables, etc. In the field of thermal anemometry, an expression for the heat loss from the cylinder is usually used to measure the velocity of the flow[2]. Since buoyancy force can significantly affect heat-transfer from the cylinder[3-5], there is a need for accurate correlations which predict the rate of heat transfer in the presence of buoyancy and at low velocities. In the present work a numerical study of laminar mixed convection from a cylinder has been undertaken.

2. Results and discussion

The angle γ made by the direction of forced flow with the gravity vector is an important parameter in studies of mixed convection[6]. Flow regimes associated with a γ of 0, 90 and 180° are, respectively, known as the parallel, contra, and the cross flow regimes.

The governing equations along with the appropriate boundary conditions have been solved using finite-difference methods. The vorticity–stream function approach and the alternating direction implicit scheme with a variable grid spacing in the radial direction have been used. The dimensionless equations governing the transient problem are given below. Here ϑ, ζ, ψ, u, v are the dimensionless temperature, vorticity, stream function, angular velocity and radial velocity, respectively *Re, Gr,* and *Pr* are the Reynolds, Grashof, and Prandtl numbers. The angles are measured as in Fig. 1

Energy

$$\frac{u}{r}\frac{\partial\vartheta}{\partial\phi} + v\frac{\partial\vartheta}{\partial r} = \frac{1}{RePr}\left[\frac{\partial^2\vartheta}{\partial r^2} + \frac{1}{r}\frac{\partial\vartheta}{\partial r} + \frac{1}{r^2}\frac{\partial^2\vartheta}{\partial\phi^2}\right] \tag{1}$$

Vorticity

$$\frac{u}{r}\frac{\partial\zeta}{\partial\phi} + v\frac{\partial\zeta}{\partial r} = \frac{1}{Repr}\left[\frac{\partial^2\zeta}{\partial r^2} + \frac{1}{r}\frac{\partial\zeta}{\partial r} + \frac{1}{r^2}\frac{\partial^2\zeta}{\partial\phi^2}\right] + \frac{Gr}{Re^2}\left[\sin(\delta-\phi)\frac{\partial\vartheta}{\partial r} + \frac{\cos(\delta-\phi)}{r}\frac{\partial\vartheta}{\partial\phi}\right] \tag{2}$$

Stream function

$$\frac{\partial^2\psi}{\partial r^2} + \frac{1}{r}\frac{\partial\psi}{\partial r} + \frac{1}{r^2}\frac{\partial^2\chi}{\partial\phi^2} = -\zeta \tag{3}$$

Velocity

$$u = -\frac{\partial\psi}{\partial r} \text{ and } v = \frac{1}{r}\frac{\partial\psi}{\partial\phi} \tag{4}$$

The non-dimensional variables are defined as follows:

$$u = u'/U_\infty,\ v = v'/U_\infty,\ = r = r'/R,\ \vartheta = (T-T_\infty)/(T_w-T_\infty),\ \psi = \psi'/U_\infty R,\ \zeta = \zeta' U_\infty/R. \tag{5}$$

Here, U_∞ and r are the free-stream velocity and the radius of the cylinder, respectively. The solution of eqns (1) through (4) together with the appropriate boundary conditions gives the desired solution. Boundary conditions should be specified on the surface of the cylinder, at 'infinity', and on the symmetry lines (when symmetry exists). The boundary condition for the temperature on the heated cylinder surface follows directly from its definition while the conditions for stream function and vorticity follow from the no-slip condition[7]. Thus, on the cylinder surface we have,

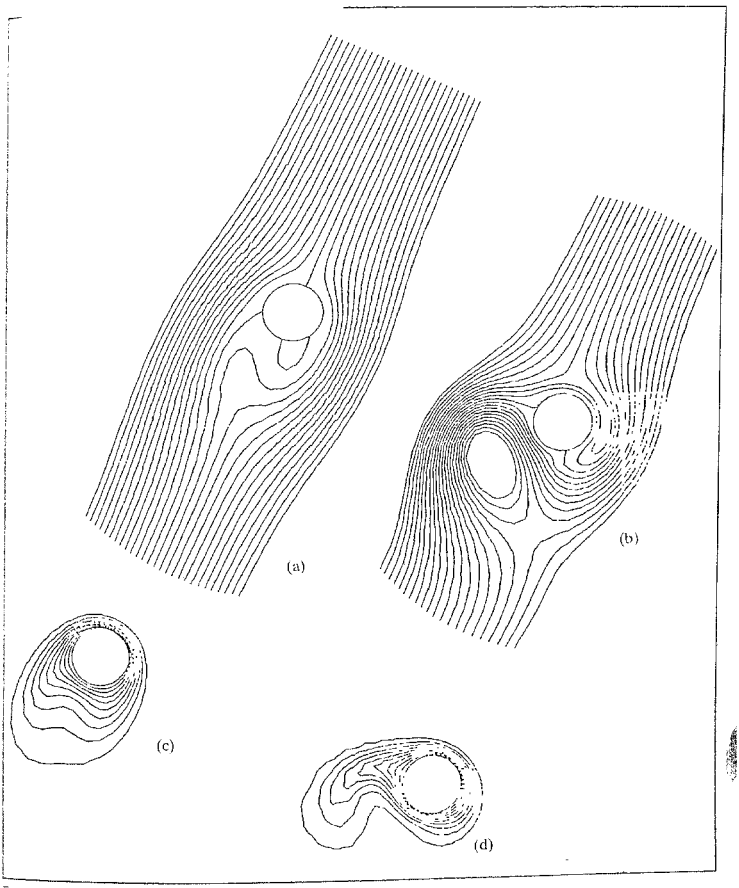

FIG 1 Geometry and nomenclature

$\vartheta = 1{\cdot}0,\ \psi = 0{\cdot}0,\ u = 0{\cdot}0,\ v = 0{\cdot}0,\ \zeta = \zeta_{wall}$, and

$\vartheta \to 0{\cdot}0,\ \zeta \to 0{\cdot}0,\ u \to -\sin\phi$ as $r \to \infty$. (6)

Symmetry about the vertical plane exists for the parallel and contra flow regimes. Hence, only one half

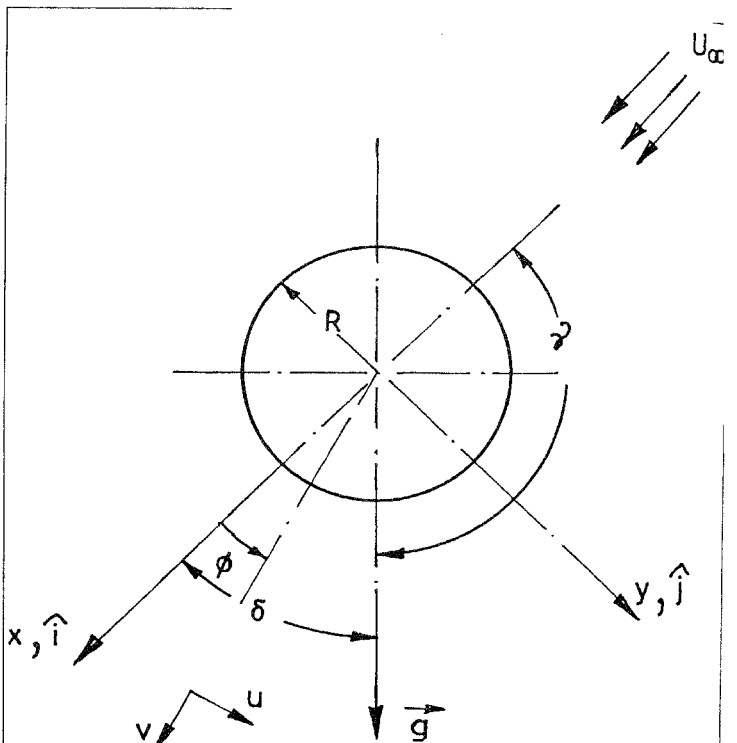

FIG. 2. Stream function and isotherm plots for $\gamma = 135°$, Re = 40, Pr = 0·73. (a) Gr = 800, (b) Gr = 8000 (c) Isotherms, Gr = 800 (d) Isotherms, Gr = 8000.

of the solution domain requires to be solved for these regimes. The following well-known boundary conditions are used for the symmetry lines.

$$\psi = \frac{\partial \nu}{\partial \phi} = u = \frac{\partial \vartheta}{\partial \phi} = 0{\cdot}0.$$

In the present work, the problem is solved for a variety of flow regimes (γ) and for different *Re*, *Gr*, and *Pr*. Figure 2 shows some sample results in the form of stream function and isotherm plots for a flow regime corresponding to $\gamma = 135°$. A general correlation has been proposed to estimate heat-transfer from the cylinder when angle γ is arbitrary. It was shown that information useful in the field of hot-wire and

hot-film anemometry can be obtained from this correlation. Since a wide variety of fluids are usually encountered in the field of anemometry, the effect of Prandtl number variation on heat-transfer from the cylinder is studied for a range of fluid Prandtl number ($10^{-2} \leq Pr\ 10^{-2}$) and correlations are proposed. The problem of mixed convection round a wire ($Re \ll 1$) was considered and correlations have been proposed to estimate heat-transfer. Finally, the problem of conjugate mixed convection around a cylinder is considered as it is of importance in the field of thermal anemometry. Results indicate that the isothermal solution can be used if the ratio of solid to liquid thermal conductivities is greater than or equal to 500.

References

1 MORGAN, V T.	*Advances in heat transfer*, Vol. 11, pp. 199–264, 1975, Academic Press.
2 COLLIS, D.C AND WILLIAMS, M J.	*J. Fluid Mech* , 1959, **6**, 357–384.
3. JALURIA, Y	*J. Appl. Mech.*, 1979, **46**, 231–233.
4 SUNDEN, B	*Int J. Heat Mass Transfer*, 1983, **26**, 1329–1338.
5 AMOUCHE, M AND PEUBE, J.L.	*Int. J Heat Mass Transfer*, 1985, **28**, 1263–1279.
6 SHAUKATULLAH, H. AND GEBHART, B.	*ASME J. Heat Transfer*, 1978, **100**, 381–382.
7. ROACHE, P J	*Computational fluid dynamics*, 1976, Hermosa Publishers, Albuquerque, USA

Thesis Abstract (Ph.D.)

Aerodynamic investigation of a mixed-flow pump by Arjun Sarathi Ray

Research supervisors: S. Soundranayagam and J.H. Arakeri
Department: Mechanical Engineering

1. Introduction

Mixed-flow turbomachines find application as circulating water pumps of power stations, diagonal flow turbines and in that region of industrial use which lies between the ranges of conventional centrifugal and axial flow machines. The aerodynamics of mixed-flow machines are particularly interesting as they are midway, displaying features of both centrifugal and axial flow This work describes an experimental investigation of flow through a mixed-flow pump in an aerodynamic test rig.

2. Experimental

The pump tested had a conical hub-type semi-open rotor fitted in a bowl casing followed by a stator guide vane row. Surveys of aerodynamic parameters have been made up and downstream of the rotor and stator blading. A method of measurement of all the three components of velocity by a single-inclined rotatable hot-wire has been successfully implemented in the present investigation. A high amplification bifluid inclined-tube micromanometer was designed and used for the measurement of low pressures.

3. Results

Measurement showed that at reduced flow rates, reversal of flow occurs near the tip upstream of the rotor and near the hub downstream. At high flow rates, the flow reverses near tip at downstream only. In fact, there is only a limited regime of operation on the characteristic curve where the flow is not reversed before or after the impeller. The best fluid-dynamic efficiency point is observed to be almost midway of this non-reversed flow regime.

The reversed flow eddy at inlet by itself is very narrow but it induces pre-swirl over a large portion of the inlet annulus. Evidence suggests that fluid particles from within the zone of reversal are entrained by and mix with the clean flow outside continuously so that the inlet flow too is essentially 'turbulent' and without any expressible circumferential regularity. Similar inferences hold good downstream of the impeller also at reduced flow rates.

The role of the relative eddy[1] in modifying the flow outlet angle in a turbomachine is most easily clarified in studies with mixed-flow configurations. The effect of it appears in the blade-to-blade plane as 'through-flow' eddy. It is shown that the effect of the through-flow eddy is extremely important and must be considered for better prediction of outlet flow angles. Other basic phenomena which influence the flow outlet angle are the tip clearance leakage flow[2], the meridional velocity change[3] and secondary flow[4]. Suitable analytical models for prediction of these effects have been discussed.

For prediction of performance of a turbomachine, one requires the capability to predict, apart from the fluid outlet angle, as also the spanwise variation of meridional velocity and loss coefficients. Through-flow solutions of the mean hub-to-tip stream surface has been carried out for the pump under consideration by streamline curvature computation technique[5] and compared with experimental results. The results of attempts for theoretical assessment of total pressure loss are compared with experimental measurements. It is seen that existing loss models are inadequate for loss prediction and further work is reqtired in this direction to be able to predict loss with reasonable accuracy in such machines.

The pattern of variation of yaw angle downstream of the stator row suggests the existence of a circulatory motion of fluid in each blade-to-blade channel of the stator, associated with the presence of axial component of vorticity downstream of the rotor row. Hence a stator, while removing the swirl shed by a rotor, may impart another swirl to the flow—the tangential component of velocity near the hub tending to be in the opposite direction to that near the casing. This belies a conjecture[6] that the flow, downstream of a stator row of any pump, will necessarily be swirl-free at the design point at the least.

The head-flow characteristic of the machine showed a droop at reduced flow rates, typical of what one usually notices in an axial flow machine with the onset of blade stall. Study of the time history of velocity downstream of rotor illustrates that, unlike rotating 'stall-cells' in axial flow machines, the blade stall in the present case does not possess any regular pattern nor any unique speed of propagation. Near the hub at downstream of rotor, where the flow finally reverses upon reduction of flow rate, the stall appears as patches of 'blockage'-type disturbance over an otherwise systematic train of blade wakes when the flow coefficient reaches a value where the droop in the characteristic curve starts.

The study reveals the possibility of estimating the overall flow pattern by using relatively straightforward methods and the necessity of more information regarding losses and their distribution for a closer prediction of the machine characteristics.

References

1. LEWIS, R.I. *Thermodynamics and Fluid Mechanics Convention*, Liverpool, 1966, Paper-29
2. LAKSHMINARAYANA, B. *Trans. ASME, Basic Engng D*, 1970, **92**, 467–482
3. SOUNDRANAYAGAM, S. *J. Mech. Engng Sci.*, 1971, **13**, 92–99.
4. HORLOCK, J.H. *AGARD Conf. Proc.*–214, 1977.
5. NOVAK, R.A. *Trans. ASME, J. Engng Power*, 1967, **89**, 478–490.
6. STEPANOFF, A.J. *Centrifugal and axial flow pumps*, 1957, Wiley.

Thesis Abstract (M.Sc.(Engng))

A personal computer base analysis and evaluation system for switched mode power converters by Sauvik Chattopadhyay
Research supervisor: V. Ramanarayanan
Department: Electrical Engineering

1. Introduction

The availability of fast-power switching devices has opened up the application of SMPS for practically all

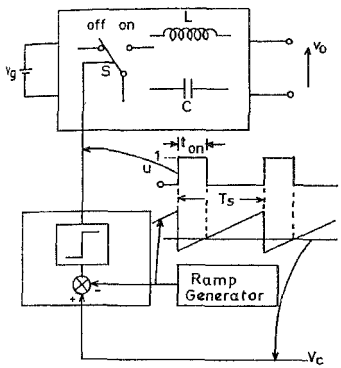

FIG. 1. A general switched-mode converter.

power supply applications. SMPS feature high efficiency, small size and weight and low cost. The operation of the basic switching converter circuits has been extensively covered in the literature[1]. Many modelling techniques such as circuit averaging[2], describing functions[3], state-space averaging[4], current-injected modelling[5], variable structure system[6], etc., have been successfully applied for the analysis of SMPS. The state-space averaging method has emerged as popular among these methods and is well suited for computer-aided analysis.

This work reviews briefly the state-space averaging method and develops a convenient formulation of the system equations suitable for computer solution. A software is developed based on this formulation, which takes input data from circuit parameters and provides the performance functions of the converter. An SMPS evaluator has been built which provides the necessary input signals such as control-input modulation, switching frequency modualtion, input voltage modulation, etc., to test any SMPS. An automated measurement system consisting of a PC, a frequency response analyser and the SMPS evaluator have been integrated for the measurement and verification of the basic SMPS performance functions. Analysis and measurement results on a few basic converters are presented.

2. Theory

A typical switched mode converter is shown in Fig. 1. The converter switches between two linear circuits in each of the switching period. Under the assumption that the state velocity (x) is constant in each of the subperiods, we may approximate the state velocity with an equivalent state velocity which is the average of the state velocities in the two different subperiods. The assumption that the state velocity is constant in each interval will be valid provided the circuit time constants[3] are much higher than the switching period. The averaged system description then is given by[8]

$$Px = [A_1 d + A_2(1-d)]\, x + [b_1 d + b_2(1-d)]\, V_g + [m_1 d + m_2(1-d)]\, i_z \tag{1}$$

$$v_0 = [q_1 d + q_2(1-d)]\, x + [k_1 d + k_2(1-d)]\, i_z \tag{2}$$

$$i_g = [p_1 d + p_2(1-d)]\, x \tag{3}$$

where d = duty ratio. Thus the averaged system eqns (1) to (3) give an approximate equivalent continuous system which may be analysed following standard state-space methods.

3. Performance functions of the converter

The system equation given by eqn (1) indicates the state velocities of the equivalent system as a function of the input variables (duty ratio d, input voltage V_g, load change i_z) and the system state x. Equations (2) and (3) give the output of the converter as a function of the state x, and input variables d, v_g and i_z.

Under steady state the converter operates with input voltage V_g, duty ratio D and load R ($i_z = 0$). The steady-state solution is then

$$X = -A^{-1}\, b\, V_g \tag{4}$$

$$V_0 = qX \tag{5}$$

$$I_g = pX \tag{6}$$

where

$$A = A_1D + A_2(1-D)$$

$$b = b_1D + b_2(1-D)$$

$$q = q_1D + q_2(1-D)$$

$$p = p_1D + q_2(1-D)$$

D = steady-state duty ratio.

The control of the converter is through the duty ratio d. Usually the converter is operated in closed loop such that the output voltage is maintained through controlling d against variations in v_g or load (R). To obtain various dynamic performance functions of the converter, the system input variables may be perturbed ($d = D + \hat{d}$, $v_g = v_g + \hat{v}_g$, $i_z = \hat{i}_z$, $x = X + \hat{x}$), and separated into steady state and small signal parts. The small signal model thus obtained may be linearised (dropping the nonlinear product terms) to obtain the following linear small signal model of the converter.

$$\dot{\hat{x}} = A\hat{x} + b\hat{v}_g + m\hat{i}_z + f\hat{d} \tag{7}$$

$$\hat{v}_0 = (q_1-q_2)\, X\hat{d} + q\hat{x} + k\hat{i}_z \tag{8}$$

$$\hat{i}_g = (p_1-p_2)\, X\hat{d} + p\hat{x} \tag{9}$$

$$k = k_1D + k_2(1-D)$$

$$f = [(A_1-A_2)X + (b_1-b_2)V_g]$$

where the hat (ˆ) indicates small signal *ac* variables. Equation (7) may be rearranged as

$$\dot{\hat{x}} = A^*\hat{x} + b^*\hat{v}_g + m^*\hat{i}_z + f^*\hat{d}\,. \tag{10}$$

From eqns (8), (9) and (10) we may obtain the following dynamic performance equations of the converter

a) Audio susceptibility $[\hat{v}_0/\hat{v}_g\ (\hat{d} = 0;\ \hat{i}_z = 0)]\ F$.

$$F = q(sI - A^*)^{-1}b^* \tag{11}$$

b) Input admittance $[\hat{i}_g/\hat{v}_g\ (\hat{d} = 0;\ \hat{i}_z = 0)]\ Y$.

$$Y = p(SI-A^*)^{-1}b^* \tag{12}$$

c) Output impedance $[\hat{v}_o/\hat{i}_z\ (\hat{d} = 0;\ \hat{v}_g = 0)]Z$.

$$Z = q(SI-A^*)^{-1}m^* + k \tag{13}$$

d) Control gain $[\hat{v}_o/\hat{d}\ (\hat{v}_g = 0;\ \hat{i}_z = 0)]G$.

$$G = (q_1-q_2)\, X + q(SI-A^*)^{-1}f^* \tag{14}$$

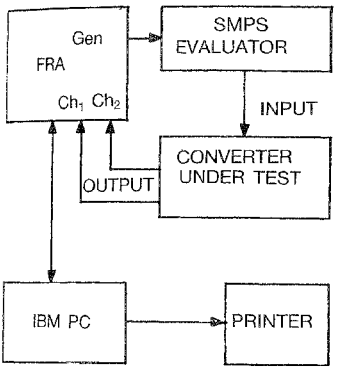

FIG 2 Test setup for computer-aided measurement of performance functions of switching converters.

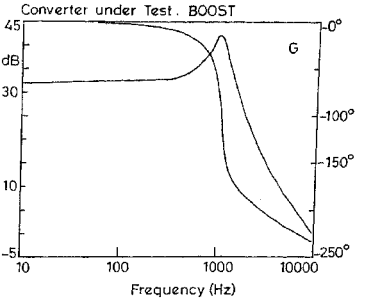

FIG. 3. Control gain of a boost converter.

4. Computer-aided analysis of converters

When the system parameters are known (P, A_1, A_2, b_1, b_2, m_1, m_2, p_1, p_2, q_1, q_2, k_1, k_2, v_g,D), eqn (4) to (6) and (11) to (14) may be used to evaluate the steady state and dynamic performance of the converter. The ON and OFF period system matrices are input to the program. The program evaluates the steady-state solution at first. Then the dynamic performance functions are evaluated as a function of frequency. The transfer functions thus evaluated are available either in normalized pole-zero form or in a more convenient Bode Plot[8].

5. SMPS evaluator

To measure the performance functions of the converter, an SMPS evaluator was built. The evaluator provides a voltage source v_g (to be used as input power for the converter under test) and a set of drive signals to be used to drive the switches in the converter under test. The steady-state switching frequency (F_s) and the duty ratio (D) may be set anywhere in the range of 20 to 100 kHz and 0·2 to 0·8, respectively. The steady-state source voltage (V_g) may be set in the range of 15 to 20 volts. Further, sinusoidal modulations may be superimposed using a signal generator on V_g, F_s and D at any frequency.

6. Computer-aided measurement of performance functions

The measurement of the dynamic performance function is done using a Schlumberger 1250 frequency response analyser (FRA). The FRA has one output channel which is a signal generator whose amplitude and frequency are controllable (0–15V; 0–64 kHz) and two input channels. To measure any dynamic performance function (say $\hat{v}_o/\hat{v}_g$), the generator output is connected to the appropriate input ($\hat{v}_g$) of the SMPS evaluator. The evaluator output v_s and drive signals are connected to the converter under test (v_o and v_g) are connected to channels 2 and 1 of the FRA, respectively. On starting the test, the FRA carries out the test and displays the measured transfer function in magnitude and phase format. By repeating the test at different generator frequencies the transfer function as a function of frequency may be generated. Since the testing involves a number of settings and repetition at different frequencies, it is well suited for automation. A resident program in the PC does the instrument settings and collects the test data. The results are displayed in the Bode Plot format so that a fast comparison with theoretical prediction can be made.

7. Experimental results

To test the effectiveness of the system, a few simple converters were built and tested. An exhaustive set of test results are already reported by Chattopadhyay and Ramanarayanan[7]. A representative frequency on a boost converter is shown in Fig. 3.

8. Conclusion

A PC-based analysis and evaluation system for switching converters has been developed and tested on simple converters for its effectiveness. Such a computer-aided evaluation facility is a great help in our future work to analyse the effect of different nonidealities in switching converters, design and study of suitable closed-loop compensators and to study scaled-down models of larger power converters.

References

1. MIDDLEBROOK, R. D. AND CUK S M. — *Advances in switched mode power conversion*, Vols I & II, 1983, TESLA Co., Pasadena.
2. WESTER, G. W. AND MIDDLEBROOK, R D. — Low frequency characterisation of switched dc-dc converters, *IEEE Trans.*, 1973, **AES-9**, 376–385
3. MIDDLEBROOK, R.D. — Describing function properties of a magnetic pulse width modualtor, *IEEE Trans.* 1973, **AES-9**, 386–398
4. MIDDLEBROOK, R.D AND CUK, S. M. — A general unified approach to modelling switching converter power stages, *IEEE Proc. Power Electronics Specialists Conf 1976, Record.* pp. 18–34.
5. CHETTY, P R.K. — Current injected equivalent circuit approach to modelling of switched dc-dc converters (discontinuous inductor conduction mode), *IEEE Trans.*, 1982, IA-18. 295–299.
6. RAMANARAYANAN, V. *et al* — Sliding mode control of power converters, *J. Indian Inst. Sci.*, 1989, **69**, 195–211.
7. CHATTOPADHYAY, S AND RAMANARAYANAN, V. — A PC-based analysis and evaluation system for SMPS, *J Indian Inst. Sci.*, 1991, **71**, 259–269.
8. BORRIE, J.A. — *Modern control systems. A manual of design methods*, 1986, Prentice-Hall.

Thesis Abstract (M.Sc.(Engng))

Algorithms for dynamic secure economic dispatch by Manoj Kumar Sinha
Research supervisors: P.S. Nagendra Rao and D. Thukaram
Department: Electrical Engineering

1. Introduction

The main objectives in power system operation are to maintain the continuity of supply and also to guarantee a certain quality of supply in the most economical way. Although it is very difficult to guarantee a secure system operation under all conditions, it can be enhanced significantly. The economic dispatch problem is a constrained minimization problem. Traditionally, the constraints considered in this minimization problem are the units' capacity limits only. However, in the recent past, it is being recognized that the scope of this function should be enlarged so as to consider some more operational and security constraints. With this enlarged scope, the economic dispatch problem can no longer be treated as static optimization problem.

static optimization problem. Instead, it becomes a dynamic one. The need of addressing the economic dispatch problem in this broader scope has been recognized as one of the unresolved problems.

2. Dynamic secure economic dispatch

The conventional economic dispatch[1,2] is aimed at meeting the instantaneous load demand in the most economical way. As the load varies continuously the units are scheduled on a point-to-point basis so as to follow the changing load. When the schedules for a forecasted load curve are obtained based on a set of instantaneous load demands, then it may not be possible to change the generation of the units as dictated by the schedules due to the constraints on the rates at which the thermal units can be loaded or deloaded. Hence, if the economic dispatch is to provide a practically viable solution, these constraints must be included in the problem formulation. The inclusion of the units' rate constraints makes the problem a dynamic one. Further, it is preferable to include the requirements of minimum spinning reserves[3] and also the constraints on station and network limits which are important in enhancing the system security into a broader economic dispatch problem. When all the above features are included with those of the conventional ones the enlarged problem can be referred to as the dynamic secure economic dispatch (DSED) problem[4,5]. Algortithms for the DSED problem must be efficient as the solutions are required in real time.

3. Contribution of the thesis

This work is essentially concerned with the development of efficient algorithm for the solution of the dynamic secure economic dispatch (DSED) problem. In the first part of the work, the problem is considered assuming linear cost functions[6]. Existing solution algorithms for this problem are in the linear programming framework. This work takes a different path. Attempts are made to develop computationally efficient heuristic algorithms, which exploit the special nature of the problem. Two types of procedures have been developed. The first is meant for determining the optimal schedule considering a subset of the specified set of constraints involving very little computations. The second is meant for systematically modifying the above suboptimal/unfeasible (in the overall context) solutions towards optimal value over a sequence of steps. At each step of the modification the algorithms seek to change the schedule so that the cost escalation is kept as small as possible.

In the second part of the work, the DSED problem is investigated assuming quadratic cost functions. The motivation for this effort is the fact that the static economic dispatch problem is invariably based on quadratic cost functions. However, except for a small attempt, there appears to have been no significant effort to formulate and solve the DSED problem considering the quadratic cost functions. The problem when formulated in this way, turns out to be a standard QP (Quadratic Programming) problem. However, attempts to solve this using a standard QP package were not very fruitful. Hence, even in this case an heuristic algorithm is developed which is similar to that of the linear cost function case.

4. Conclusions

The algorithms developed in this work to solve the DSED problem (assuming linear and quadratic cost functions) have been tested on different systems. The results are presented and are compared with those obtained by the earlier approach. The comparison shows that these QP methods are more efficient and could be applied for large systems.

References

1. HAPP, H.H. — Optimal power dispatch–A comprehensive survey, *IEEE Trans.*, 1977, **PAS-96**, 841–854.

2. IEEE Working Group Report — Description and bibliography of major economy security functions, Parts–I, II & III, *IEEE Trans.*, 1981, **PAS-100**, 211–235.

3. WOOD, W.G. — Spinning reserve constrained static and dynamic economic dispatch, *IEEE Trans.*, 1982, **PAS-101**, 381–388.

4. IRVING, M.R. AND STERLING, M.J.H. — Economic dispatch of active power with constrained relaxation, *IEE Proc., Gen. Transmission Distribution*, 1983, **130**(4), 172–177.

5. HINDI, K.S AND GHANI, M.R. AB — Multiperiod secure economic dispatch for large scale power systems, *IEE Proc. (C), Gen. Transmission Distribution*, 1989, **136**(3), 130–136

6. NAGENDRA RAO, P S., SINHA, K M. AND THUKARAM, D. — Dynamic secure economic dispatch–New algorithm, *Proc. VI NPSC*, 1990. IIT, Bombay.

Thesis Abstract (M.Sc.(Engng))

Multifactor ageing of high-voltage rotating machine stator insulation by M.B. Srinivas
Research supervisor: T.S. Ramu
Department: High Voltage Engineering

1. Introduction

Modelling and analysis of insulation failure due to ageing under multifactor stress is a subject of considerable current interest. Various phenomenological models have been suggested from time to time to describe the long-time behaviour of insulation systems and some of them are still being used to estimate the life of insulation[1,2]. Also, diagnostic test procedures exist for monitoring the status of insulation during service.

The contribution of the present work is two fold. The first is the development of a phenomenological multifactor stress model for predicting the life of electrical insulation under the combined action of electrical, thermal and mechanical stresses. This model has been tested using the ageing failure data on high-voltage rotating machine stator insulation. The second contribution includes the development of a diagnostic test method for assessing the level of degradation of rotating machine insulation in service using the results of partial discharge pulse/magnitude data. A possible method of predicting the useful remaining life has also been suggested.

2. Theoretical

Several aspects of insulation ageing under combined electrical and thermal stresses have been covered earlier[1-3]. The model for failure of insulation in the presence of mechanical stresses can be shown to be an inverse power law, similar to the electrical failure model.

2.1 *Multistress model*

The insulation life at any electric stress E and at room temperature can be expressed by the empirical power law thus,

$$L = KE^{-n} \tag{1}$$

in which K and n are constants.

When thermal and mechanical stresses are also present in addition to electrical stress, the power law constants can be treated as functions of T and S and the above expression should be weighed by thermal and mechanical ageing terms thus:

$$L(E,T,S) = K(T,S)\ E^{-n(T,S)} \exp(B/T)\ S^{-m}\ . \tag{2}$$

Now, if E_0, T_0 and S_0 are the operating stresses, then,

$$L_0 = L(E_0,\ T_0,\ S_0)\ K(T_0,\ S_0)\ E^{-n(T,S)} \exp(B/T_0)\ S_0^{-m}\ . \tag{3}$$

By virtue of the phenomenological fact that the endurance coefficient is a decreasing function of other supplementary stresses T and S, and assuming, as first approximation, that the interaction between these stresses is small, it is possible to express $n(T,S)$ as a linear combination of the endurance coefficients when the thermal and mechanical stresses are present separately with electric stress as:

$$n(T,S) = n(T) + n(S). \tag{4}$$

Table I
Comparison of experimental and estimated lives

Ageing stresses			*Estimated life**	*Experimental life***
T *t°C)*	*U* *(kV)*	*M* *(kg/cm²)*	*(hours)*	*(hours)*
180	20	0	1558	1400
180	24	5·52	186	190
210	20	0	643	680
210	26	5·52	77	80
230	20	0	290	200
230	26	6·64	24	25

* See eqn. (7).
** extracted from the corresponding Weibull plot.

Table II
Coefficient of correlation between diagnostic properties, breakdown voltage, U_d and the stress factor, G

Parameter	*G*	*Δ tan δ*	*Δ C/C*	E_{pd}	R_{dc}	U_d	Sk
G	–	0·4483	0·2861	0·4692	−0 2778	−0·9429	−0·9472
Δ tan δ	−0·4483	–	0·9282	−0·2210	−0·9556	−0·6462	−0·5725
Δ C/C	0·2861	0·9282	–	−0·5509	−0·9943	−0·4181	−0·3249
E_{pd}	0·4692	−0·2210	−0·5509	–	0·4971	−0·4845	−0·5678
R_{dc}	−0·2778	−0·9556	−0·9943	0·4971	–	0·4412	0·3505
U_d	−0·9429	−0·6462	−0·4181	−0·4845	0·4412	–	0·9949
Sk	−0·9472	−0·5725	−0·3249	−0·5678	0·3505	0·9949	–

Also, it is known phenomenologically that $n(T)$ and $n(S)$ are decreasing functions of T and S, respectively, thus:

$$n(S) = a - bS$$

$$n(T) = c - d/T. \tag{5}$$

When S is very small or zero and T is less than or equal to the room temperature, then $n(T,S)$ is given by,

$$n(T,S) = a+c = n_0 \text{ (say)}. \tag{6}$$

Therefore, life L can be written as,

$$L = L_o \cdot K(T,S) \cdot \left(\frac{E^S}{E_0^S}\right)^b \cdot \left(\frac{E}{E_0}\right)^{-n_0} \cdot \left(\frac{E^{1/T}}{E_0^{1/T}}\right) \cdot \left(\frac{S}{S_0}\right)^{-n_1} \cdot$$

$$\exp\left\{\frac{\Delta GE}{K}\left(\frac{1}{T}-\frac{1}{T_0}\right)\right\}.$$

To determine the constant in the above equation, experiments have to be conducted at single electric, thermal and mechanical stresses, combined electrical and thermal stresses and combined electrical, thermal and mechanical stresses.

3. Experimental

The specimens for ageing experiments have all been derived from full size 11 kV rotating

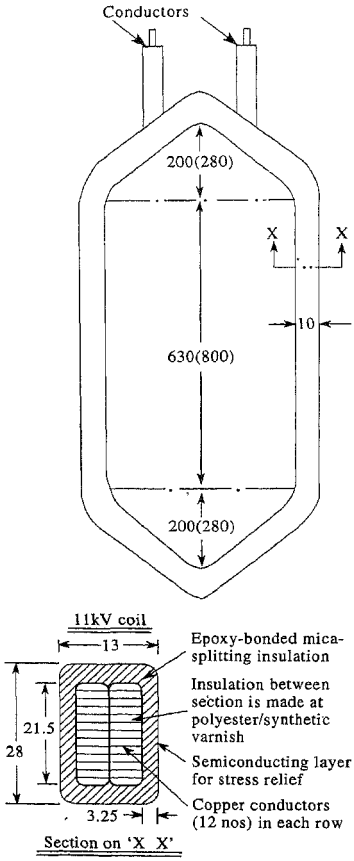

FIG. 1. Full-size coil geometry (all dimensions are in mm).

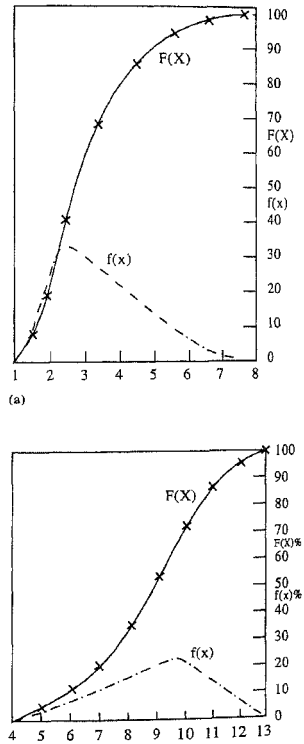

f(x) = density function, F(X) = distribution function

FIG. 2. Statistical distribution of pulse counts after (a) 500 hours, and (b) 3000 hours of ageing.

machine stator coils shown in Fig. 1. The edges of the conductors were rounded off longitudinally to radii at which the electric stress concentration is a minimum. In running the ageing experiments, two types of specimens were used: (i) full-size coils, and (ii) short lengths of coils derived from the above. Full-size coils have been used in all experimental runs where vibrational (fatigue) stresses have been applied. However, when the mechanical stresses were not applied, shorter lengths of coils have been used. Experiments were conducted both under single and multifactor stress conditions.

4. Results and discussion

The times to failure of overhang insulation under combined electrical, thermal and vibration (fatigue) stresses are assumed to follow a two-parameter Weibull distribution since the degradation is a weak link process. The parameters of distribution were estimated using maximum likelihood estimation technique. These parameter estimates were in turn used to arrive at the values of model constants. Table I compares the life estimates using the suggested model with experimentally obtained lives. As can be seen, the lives obtained using the model are quite close to the experimental lives.

As mentioned earlier, a diagnostic test method has been proposed based on diagnostic measurements such as incremental loss tangent, capacitance change, partial discharge pulse count/magnitude and PD energy carried out on machine insulation. These measurements have been correlated with dielectric strength of insulation. Table II presents correlations between them. While some properties correlate well with dielectric strength, others do not. For example, dc resistance and $\Delta C/C$, $\Delta \tan \delta$ and $\Delta C/C$ are well correlated.

A second and more interesting observation was made when partial discharge pulse amplitude distributions were plotted as functions of time. As can be inferred from Fig. 2, at the beginning of the ageing period, the distributions were skewed to the left. As ageing progressed, the skewness approached zero. Further ageing would make the density function skewed to the right. Failure invariably occurs after this condition is reached. As can be seen from Table II, the correlation coefficient between skewness and loss of dielectric strength is very high ($> 0{\cdot}9$).

6. Conclusions

The work reported provides a means of estimating life as well as assessing the level of degradation of high-voltage machine insulation under multifactor stress. The constants of inverse power law are treated as functions of thermal and mechanical stresses. These constants can be obtained by conducting single as well as multistress ageing experiments, which in turn can be used to obtain life at any stress or stresses. The diagnostic test procedure proposed makes use of skewness of partial discharge pulse amplitude distribution as a measure of degree of deterioration of machine insulation.

References

1. RAMU, T.S. — On the estimation of life of power apparatus insulation under combined electrical and thermal stresses, *IEEE Trans.*, 1993, **EI-20**, 70–78.

2. SIMONI, L. — Life models for insulating materials under combined thermal-electric stress, *Colloquim of Professional Committee of IEE, Group-52*, pp 1–10, Dec. 1980.

3. FALLOU, N. AND BURGIERE, C. — First approach on multiple stress accelerated life testing of electrical insulation–*Annual Report, CEIDP, NCR Conf.*, Pocono, October 1979.

Thesis Abstract (M.Sc.(Engng))

Development of ratio-transformer-based self-balancing ac bridge for very low capacitance measurements by C. Nagaraja Murthy
Research supervisor: M.V. Lele
Department: Instrumentation and Services Unit

1. Introduction

The accurate measurement of low-capacitances using conventional bridges in the presence of stray and

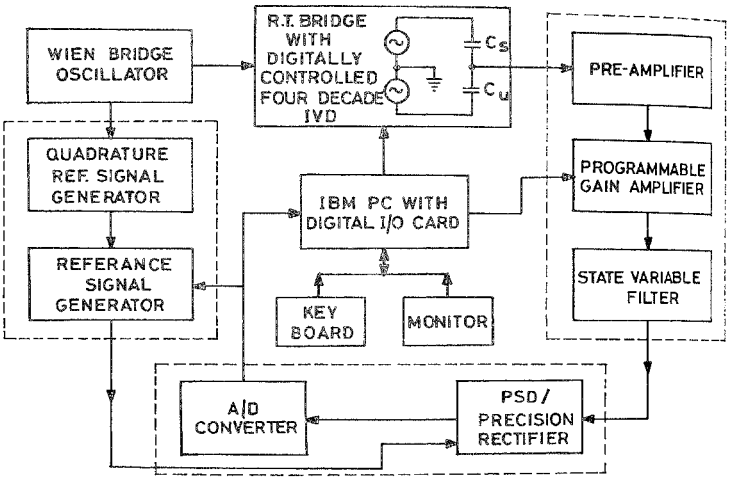

FIG. 1 Functional block diagram of self-balancing ratio-transformer bridge.

ground capacitances is very cumbersome. This problem can be solved by using a three-terminal capacitor and a ratio-transformer impedance bridge. Although these bridges provide good resolution and accuracy in measurements, manual balancing hardly meets today's requirement for speed of measurement and automation. An attempt has been made to design and construct a ratio-transformer-based self-balancing ac bridge for the measurement of low capacitances having a resolution less than 1 part in 10^5.

2. Functional description

Figure 1 represents the functional block diagram of the self-balancing ratio-transformer bridge. The details of the building blocks of the system are described here.

A Weinbridge oscillator having a good frequency (1kHz) and amplitude stability is used for the excitation of the bridge. The heart of the bridge is a four-decade inductive voltage divider (IVD) wound on a high permeability (1×10^5) super mumetal core. The universally accepted technique of winding IVDs developed by Hill and Miller[1] has been used here. This winding technique on a high permeability core ensures equality of coupling between all sections of the windings and makes them virtually ideal ratio arms. DIP-type reed relays having very low-contact resistance have been used for the selection of the ratio tappings. The decoder logic to activate these relays is implemented using digital ICs. The unknown capacitor Cu and the standard capacitor Cs are connected as shown in the figure. The output of the bridge is fed to a lock-in-amplifier detector, comprising a pre-amplifier, programmable gain amplifier and a state variable filter as the front end of the detector. The output of the filter and the output of the quadrature reference generator is fed to PSD through a reference signal selector circuit. The output of the PSD is digitised using an A/D converter and is fed to the computer. The personal computer under the software control adjusts the voltage ratio tappings using the relays for the balance of the bridge and then the 'Comparison'[2] or 'Intercept' technique is applied for computing the value of the unknown capacitor.

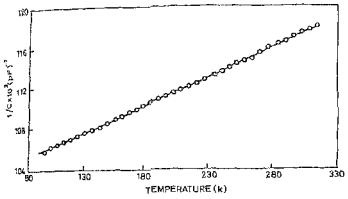

FIG. 2. Variation of I/C with temperature for germanium

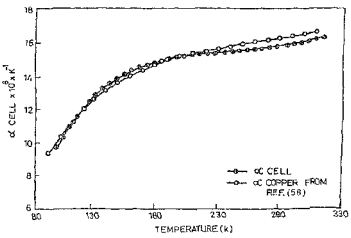

FIG. 3. Variation of cell constant (α cell) with temperature.

3. Experimental results

The accuracy of comparison and self-consistency in winding and inter connections of the ratio-transformer is determined using Hillhouse and Kline[3] method and is found to be accurate within 5 parts per million. The bridge utility has been illustrated with the help of the capacitance transducer experimental arrangement for measuring small displacements. The bridge is found to be very sensitive for the measurement of displacements less than a fraction of a micron.

The self-balancing bridge has also been used for measuring the cell constant, *i.e.*, the thermal expansion coefficient of OFHC copper in the temperature range of 90 to 340 K by taking germanium as a standard sample in the capacitance cell assembly. Figure 2 represents the variation of I/C with temperature for germanium and Fig. 3 shows the variation of cell constant (thermal expansion coefficient of OFHC copper) with temperature. It can be seen from Fig. 3 that the results are accurate within 5% of the reported values in the literature for OFHC copper[4]. Finally, the present system provides a facility for the automation of a system which requires precise and accurate measurement of low capacitances in the presence of ground capacitances or to measure any parameter which can be converted into capacitance change.

References

1. HILL, J.J. AND MILLER, A.P. — *Proc. Instn Elect. Engrs* (GB) *B*, 1962, **109**, 157–160.
2. HENRY, P.H. — *IEEE Trans.*, 1980, **IM-29**, 337–341.
3. HILLHOUSE, D L. AND KLINE, H.W — *IRE Trans.*, 1960, I-9, 251–257.
4. LEKSINA, I.E. AND NOVIKOVA, S.I. — *Thermophysical properties of matter*, The TPRC Data Series, Vol. 12, p.90, 1975, Plenum.

Thesis Abstract (M.Sc.(Engng))

Knowledge-based interpretation of remote-sensing data by L. Chandra Sekhara Sarma
Research supervisor: V.V.S. Sarma
Department: Computer Science and Automation

1. Introduction

The art and science of relating image characteristics to real-world objects and phenomena is called image interpretation. This involves examining images for the purpose of identifying objects and judging their significance for a given application. Remote-sensing satellite images with reference data provide a basis

for extraction of information for various purposes such as land use/land cover mapping, hydrology, geology, and geography[1].

Visual interpreters study remotely sensed data and attempt to identify corresponding physical objects/phenomena through logical processes[2]. Complementary to visual interpretation are computer-assisted digital techniques which are in operation are totally dependent on multispectral characteristics of individual pixels of an image[3]. However, image interpretation is more than reading and manipulating individual pixels as it involves spatial, structural and temporal aspects and articulating heuristic knowledge acquired by experience. Core activity of interpretation can be described as plausible combination of pieces of evidential information from various sources such as images, collateral data and experimental knowledge. This activity is more in the nature of explorative and qualitative reasoning in the line of artificial intelligence (AI) and expert systems (ES). AI techniques have given a boom to the development of intelligent image interpretation systems.

2. Contribution of the thesis

In this work, we review well-known operational digital techniques for classification of images and highlight their inadequacies for automatic image interpretation to meet expert-level performance. Further, we focus on knowledge-based approaches to remote-sensing image interpretation and demonstrate the application of a knowledge-based methodology for image interpretation of standard false colour composite (FCC) using Dempster–Shafer theory of evidence. The underlying assumption in our approach is that human-like interpretation is a form of intelligence-computation involving qualitative reasoning.

We analyse the knowledge elicited in the application theme of land use/land cover mapping from the experts available at the National Natural Resources Management Systems Office, Department of Space, Bangalore, and identify the types of knowledge in the domain of image interpretation. This analysis is helpful in deciding the choice of knowledge representation scheme, uncertainty handling scheme and reliability and performance analysis[4,5].

Knowledge representation is of key importance in the development of any knowledge-based system. We carry out studies on the suitability of image data base management system (IDBMS) based on relational data model[6] to serve the purpose of representing feature-oriented image knowledge. Our studies reveal that the static storage model provided by the classical relational model is inefficient in capturing the abstraction at various levels of spatial resolution. We find that structural limitations, lack of semantics and extension capability are the major disadvantages of IDBMS based on relation data model for using them as a basis for knowledge-based approaches to image interpretation. As an alternate approach, we have conceptualized detectable image objects as region/area, line and point objects. This helps in abstraction at various spatial resolution levels and provides a basis for integration with the geographical information system (GIS). The conceptualization suggests that object-oriented approach for the representation of these objects is the natural and appropriate choice. Feature values of these objects are stored in a flexible storage structure using property lists. Heuristic information is stored in the form of rules.

Reasoning is of paramount importance in any intelligent analysis activity and thus plays a key role in obtaining best possible results of interpretation. We view image interpretation as a data fusion activity in which each interpretation key is treated as a knowledge source providing evidence to formulate a unique identification name in combination with other interpretation keys for the object under study. Since the feature values represented by interpretation keys are fuzzy human expressions, we take user's confidence in describing a feature into account to handle the uncertainty.

We explore and demonstrate the possibility of using Dempster–Shafer (D–S) theory of evidence[7] to combine the evidence from various interpretation keys for interpretation of standard FCC of IRS 1A. Basic probability assignment, a representative of apportioned user belief in a proposition, is the basis for evidence combination. Unlike Bayesian method, D–S theory of evidence provides an evidential interval with support and plausibility. With this user's ignorance can be carried forward till the end of processing in a structured manner and user has choice to distribute his belief to any element or subset of identification names. Dempster's combination rule tries to discard conflicts by way of normalization and brings out consensus.

3. Performance evaluation

A prototype expert system has been developed implementing the above schemes on IBM PC in GC LISP with a view to evaluate the performance of the system. In this, we have bifurcated the given image into mutually exclusive logical objects. Two methods of calculating basic probability assignments, namely, system method and confidence method have been attempted. These methods are combined with (without) 'learning' using (not using) Dempster's rule of combination. Thus eight options arise. Three IRS-1A FCCs containing coastal belts and vegetation covers have been analyzed exploring all the eight options using this system. Analysis of the results is done with various threshold values of plausibility, belief and evidential intervals. The results of identification are compared with human expert's opinion and found satisfactory. Explanation facility is provided by tracing the rules fired in the sequence. Online storage of data about new image objects found on the image has been provided so that the image base gets updated for future enquiries.

4. Conclusions

We observe that the time taken to reason with objects represented in property lists is significantly large when compared with the if.. then rule form. Though we have taken standard FCC of IRS-1A for identification and analysis of results, the system can also be used to interpret black-and-white image or any other photographic data product for which experts can design an interpretation key. In an abstract sense, the reasoning process in our system is analogous to that of human interpreter. Because of this, we feel that this knowledge-based approach brings skilled interpreters closer to computer-assisted classification aids.

References

1. FLOYD, F.S. — *Remote sensing principles and interpretation*, Second edn, 1987, W H. Freeman
2. — *NNRMS, Image interpretation key for Landsat thematic mapper false colour composite for urban land cover and land use information*, Report No. ISRO-NNRMS-SP-24-86, ISRO Hq, Bangalore, October 1986
3. ARGIALAS, P D. — Computational image interpretation models. An overview and perspective, *Photogrammetric Engng Remote Sensing*, 1990, **56**, 871–876.
4. HAYES-ROTH, F. — Towards benchmarks for knowledge systems and their implications for data engineering, *IEEE Trans.*, 1989, **KDE-1**, 101–110
5. NORONHA, S J. AND SARMA, V.V.S. — Knowledge-based approaches for scheduling problems: A survey, *IEEE Trans.*, 1991, **3**, 160–171.
6. TAMURA, H AND YOKOYA, N. — Image database systems: A survey, *Pattern Recognition*, 1984, **17**, 29–43.
7. THOMAS, G D., LOWRANCE, J.D. AND FISCHLER, A. — An inference technique for integrating knowledge from disparate sources, *Proc. Int. Jt Conf. on Artificial Intelligence '81*, 1981, pp. 319–325.

Thesis Abstract (M.Sc.(Engng))

Downward trimming of thick film resistors by T. Badrinarayana
Research supervisors: M. Satyam and K. Ramkumar
Department: Electrical Communication Engineering

1. Introduction

Trimming is the process of adjusting fabricated resistor to the required value. So far the resistors are trimmed upwards by removing the material from certain regions by various methods like ultrasonic, air abrasive[1], laser[2] and electron beam trimming. A process of reducing the resistance by transforming the structure of the thick film resistors of both types, namely, (1) Frit glass-based ruthenium oxide resistors, and (2) Polymer-based resistors, are studied and is reported here.

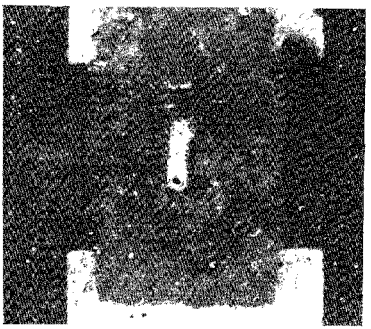

FIG 1. SEM photograph of laser-trimmed resistor

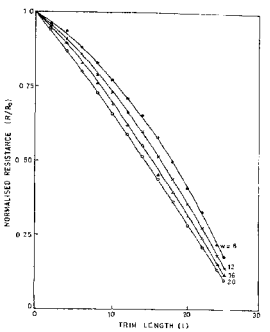

FIG 2 Typical variation of normalized resistance with tri length in resistor analogue

2. Experimental work

Resistors, of glass as well as polymer type, are screen-printed on alumina and glass epoxy substrates respectively. They are processed using standard thick film technologies applicable in each case. The fr glass-based resistors are trimmed downwards by exposing them to laser radiation in the form of track between the electrodes. The polymer-based resistors are trimmed downwards by exposing the entire resistc to infrared radiation for a certain time. The details of the trimming are given below.

2. Trimming of frit glass-based resistors

A CW argon ion laser with an output power of 4 watts was used in trimming these resistors. The bear diameter was adjusted to the required diameter by using a lens and the resistor to be trimmed was move at constant speed along its length in a direction perpendicular to the beam. At this rate of movement an power density it was found that the material had not evaporated but got transformed leading to lowe resistance values. This is due to the formation of high conductivity tracks possibly through the segregatio of conducting phase from the paste. An SEM photograph of a trimmed resistor is shown in Fig 1.

2.1 *Design of trimming tracks*

The trimming tracks are designed using resistor analogue[3] consisting of discrete resistors, of value 3- kiloohms each, connected in the form of a network. Electrodes are formed such that the number of row are proportional to the width and the number of columns are proportional to the length of the resistor Trimmed portion of the resistor is simulated by shorting appropriate rows and columns in the network The variation of resistance with increase in trim length is measured for different resistors and it is found that the resistance decreases with increase in trim length. Typical variation of normalized resistance with trim length for different track widths (W) is shown in Fig 2. Using these curves one can design trimming tracks to get the required decrease in resistance. These tracks can also be designed using computer simulation as described below. In this method, the potential distribution in a resistor is calculated by finding solution to Laplace's equation using a finite difference technique with an applied voltage of 1 volt across the resistor. The current flowing through the resistor has been then computed which essentially gives the conductance of the resistor.

3. Trimming of polymer resistors

Polymer resistors are trimmed by exposing them to infrared radiation for short periods like 4, 6 and seconds. It is found that the value of resistance decreases in each cycle of exposure to IR radiation. I

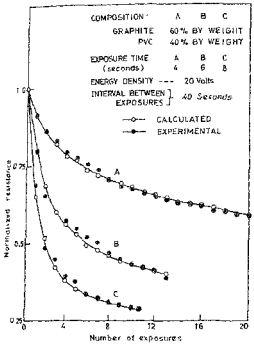

Fig. 3. Typical calculated variation of normalized resistance with number of exposures for different exposure timings.

also decreases with increase in voltage applied to the IR source, with exposure time and with the number of exposures. This behaviour is observed in resistors with different compositions. A design method has been arrived at through the understanding of the mechanism.

3.1. *Proposed mechanism*

It is known that polymer films contain cavities which start shrinking when the polymer is subjected to a temperature which is above the glass transition temperature. The rate of cavity shrinkage is found to depend on the viscosity and surface tension of the polymer at that temperature. As the cavity size decreases with time, the effective cross-section for the current increases and the resistance decreases. Since the temperature of the film depends on the voltage applied to the IR source, the time of exposure, the number of exposures and on the interval between the exposures, the change in resistance is also expected to depend upon these parameters. A model has been proposed through which the percentage change in resistance can be estimated in terms of number of exposures, duration of exposures, etc. Typical measured and calculated variation of the normalized resistances with the number of cycles is shown in Fig. 3 for resistors with different compositions. From this, one may obtain the radiation exposure schedule to get the required change in resistance.

References

1. CAPDEVILLE, M J. *Proc. Microelec. Symp.*, 1968, p.D11.
2. HEADLEY, R.C. *IEEE Proc. Elec. Comp. Conf.*, 1973, p 47.
3. SATYAM, M. *Electron devices*, 1972, p.21, Tata McGraw-Hill.

Thesis Abstract (M.Sc.(Engng))

A design environment for layout module generators by Govind T. Chari
Research supervisors: Priti Shankar and A. Prabhakar
Department: Computer Science and Automation

1. Introduction

Productive design frameworks based on structured design methods for high-density and high-performance

very large scale integrated (VLSI) circuits are still evolving. The search for structured design methods had naturally led to the use of design languages as formal notations for descriptive purposes. The thrust in research on language-based approaches to IC design came with the coining of the term silicon compilation which was first used to describe the concept of assembling parameterised pieces of layout. Today this popular term has a much larger and broader connotation. Parameterised description of layout entities are more commonly known as layout module generators.

The use of module generators and the resultant procedural approach to layout design is considered practical and suited for an open-ended layout design framework. This work reports our efforts towards the design and implementation of a design environment for layout module generators. The implementation constitutes a case study and is meant to provide an interactive and incremental style of layout design. As part of this effort a critical review of the various layout design approaches, including attempts to use language-based approach in layout design, has been done. Using a suitable taxonomical scheme, our perspective of the trends in these design approaches is presented through which the relevance of procedural approach to layout design is established.

2. Motivation

The issues involved in the design of layout module generator specification language and the provision of a system for design of module generators is described. A survey of the available literature on related efforts in this area such as ICL[1], ALI[2], SAM[3], GDT[4], ICEWATER[5], etc., has been done. It is found that the acceptance and success of generator design tools (GDT) is mainly due to its graphical design interface and the common database approach for various tools within the design system. These aspects of a design environment for module generators, which resemble programs, motivated us to investigate the possibility of extending and utilising the principles of software development environments. An alternate approach to provide an integrated design environment with graphical interface is elaborated. Considerations and various decisions involved in deriving the system architecture and the issues related to the design of module generator specification language are carefully analysed. The choice of the generator specification language constructs and a basic system configuration of the design environment are described in detail. The layout module generator specification language proposed is an extension of the C programming language.

3. Implementation

Implementation details of the basic system configuration of the design environment are discussed. The current implementation of the basic system comprises the source description translator module, the object manager module, the interpreter module, the design rule checker module and the display module. The environment supports a subset of the C programming language augmented by the constructs for layout module generator description, and has the following features:

(a) It uses the abstract syntax tree as the intermediary code. The choice of intermediary form has been influenced by the decision to allow for a tree-based editor to be incorporated.

(b) It uses the compile-load-interpret technique. The interpretive mechanism provides for incremental execution with breakpointing and design tracing facility.

(c) The execution mechanism is also supported by an online design rule checker and various run time support facilities.

Illustrative examples of some layout module generator specifications and layouts generated through them, using this system, are also presented.

The current implementation demonstrates the applicability of our approach for constructing an integrated interactive design environment for layout module generators. Enhancements required to incorporate all the C language constructs are explained. The design of a structure-oriented editor to provide a full graphical programming environment is briefly described.

Finally, a comparison of relevant aspects of this approach with similar aspects, as reported in the literature, of other generator design systems is made. The advantages of our approach are also highlighted.

References

1 AYERS, R.F *VLSI silicon compilation and the art of automatic microchip design*, 1983, Prentice-Hall.

2 LIPTON, J ALI–A procedural language to describe VLSI layouts, *Proc 19th Design Automation Conf.*, 1982, pp. 467–473.

3 TRIMBERGER, S Combining graphics and layout languages in a single interactive system, *Proc. 18th Design Automation Conf.*, 1981, pp. 234–239.

4 BURICH, M. Programming languages make silicon compiler a tailored affair, *Electronics Des.*, Dec. 1985, 134–142.

5 POWELL, P.D ICEWATER language and interpreter, *Proc. 21st Design Automation Conf*, 1984, pp. 98–102.

Thesis Abstract (M.Sc.(Engng))

Analysis of the end-to-end performance of integrated services networks by T.V.J. Ganesh Babu
Research supervisor: Anurag Kumar
Department: Electrical Communication Engineering

1. The model

In this work, we analyse end-to-end packet delays in integrated services networks that combine circuit and packet-switched traffic. We consider a network comprising switching nodes and transmission links. Each link has a number of full duplex channels that are shared by circuit and pocket-switched traffic. The well-known movable boundary scheme[1] is used to share the channels. Hence, as far as circuit traffic is concerned, we just have a circuit switching network with channels dedicated for circuit traffic. We assume uniform traffic for circuit and packet arrivals on all the node pairs. Fixed routing for circuits and packets is assumed. Routing for circuit and packet traffic is defined by the same routing matrix.

2. An approximate analysis method

With static routing and the uniform traffic assumption, we can calculate the probability at each link that all the circuit channels are busy. Next we calculate the composite arrival rate of packets at each link, from the routing matrix and the packet arrival rates for all the source-destination pairs. Next we consider each link in isolation, and assume that the blocking probability of circuit channels on the link is due to an independent Poisson circuit arrival process to the link. Further, we assume that the composite arrival process of packets to the same link is Poisson with arrival rate as calculated above. We now have an analysable model that can be used to obtain the approximate mean delay for packets at that link in the network. The approximate end-to-end mean delay of packets on a route will be the sum of the mean delays on the links constituting that route.

In a general circuit switching network, if there is a unique route between each source–destination pair then the stationary joint distribution of the number of circuits between source–destination pair is in a product form[2,3]. For simple networks, with uniform traffic for circuits, it is possible to calculate the blocking probability of each link directly from the product-form solution. For networks with a *single full duplex* channel on each link, the problem of calculating link blocking probabilities can be expressed in terms of a number of path-counting problems on the connectivity graph of the network. This calculation is carried out for N-node tandem networks and for the 2d hypercube network.

3. Numerical results (approximation and simulation): Single channel per link

The approximation technique is used to obtain mean end-to-end packet delay. We have used regenerative simulation[6] to obtain the estimates and confidence intervals for the exact values.

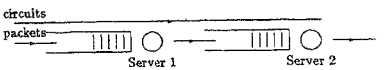

FIG. 1. A two-link integrated services model with two link circuits (Model I).

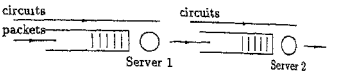

FIG. 2 A two-link integrated services model with single link circuits (Model II).

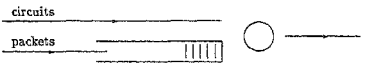

FIG. 3. Approximate model for the second link of both models in Fig. 1 and 2 (Model III)

Since a tandem network is not homogeneous (as is the hypercube network), the mean packet delay on each link has to be estimated individually, in order to estimate end-to-end mean packet delay. Since the load on the central link(s) is the maximum, we, however, only maintain regeneration statistics for the central link(s). The simulation is run until an adequately narrow confidence interval is obtained for the central link(s). From the simulation results and the corresponding values obtained from the approximate analysis, we make the following observations:

(i) At low packet occupancy and circuit occupancy, the approximation overestimates the mean packet delay.
(ii) For a particular packet load as the circuit occupancy increases from a low to a high value, the approximation overestimates at low-circuit occupancies and underestimates at high-circuit occupancies.
(iii) At low-circuit occupancy, the overestimation by the approximation increases as we move from left to right downstream along the network.
(iv) As circuit occupancy increases, first the approximation underestimates at upstream links and overestimates at downstream links, and at even higher circuit occupanices the approximation underestimates at all links.

From the simulation results and the corresponding approximation values for end-to-end mean packet delay in a 2d hypercube, we draw almost the same conclusions as we have done for the tandem network case, *i.e.*, the approximation overestimates under low-circuit occupancy and packet load, and as circuit occupancy increases, we see the tendency of underestimation even though it is not as significant as in the tandem network case. Note, though, that the routing on the hypercube is such that some links receive only Poisson packet arrivals. Thus, the approximation will not underestimate significantly even under large circuit loads.

We then attempt to explain these observations.

4. A detailed study of the approximation

We simualte two simple models. In both the models, there are two single-server queues in tandem. Packets entering the queue of Server 1, after finishing their service, will enter the queue of Server 2. In the first model (say Model I), circuits arriving will seize both servers simultaneously. In the second model (say Model II), the servers will be seized by independent circuit arrivals and no arriving circuit can seize both servers. The approximate model for link 2 in both the models is the same as the isolated link model with single channel that integrates circuit switched traffic and packet switched traffic and implements movable boundary scheme (say Model III). We compare the simulation estimates of mean delay experienced by packet at Server 2 of both models with the results obtained by analysing the approximate model for link 2.

Let S_I and S_{II} be the random variables representing the sojourn times of packets at Server 2 of Models

I and II, respectively. Let S_{III} be the random variable representing the sojourn time of packets at the single serve of Model III. Then, these results suggest that

$$E(S_I) \leq E(S_{III}) \leq (S_{II}).$$

Note that the first link has the same stochastic behaviour in Models I and II. The packet departure process from Server 1 of both the models is bursty. This is because the interdeparture times of packets from Server 1 have a coefficient of variation greater than 1, and the successive interdeparture times are correlated (which we have proved along the lines of Burke[5]). The observed inequality thus suggests that if there are *multiple link circuits* then the approximation tends to *overestimate* the packet delays, whereas if there are only *single link circuits* then the approximation tends to *underestimate* the packet delays at the second link of the 2-link model.

Note, however, that the bursts in the packet departure process from Server 1 occur because packets accumulate while a circuit holds the server, and are released in a burst when the circuit terminates. In Model I, this burst of packets will find the second server free of any circuit, whereas in Model II there is a probability that this burst of packets will again encounter a server occupied by a circuit. Thus in Model I, there is a correlation between server availability and bursts in the arrival stream, which helps in reducing delay even below that in Model III. On the other hand, the combined effect of a bursty packet arrival process and uncorrelated circuit arrivals makes the delay at node 2 in Model II exceed that in Model III.

Using the path-counting techniques for networks with single full duplex channel on each link it can be proved that the mean number of active circuits in the network is an increasing function of the offered load per route, *i.e.*, the average number of active circuits increases as the load increases. This suggests that for large loads, the number of links per active circuit should decrease as load increases. It can be proved that the average length of the active circuits approaches 1 as the offered load per route goes to infinity. From these results, we make the following conjecture: the average length of active circuits is a decreasing function of the offered load per route. This conjecture is tested and found true for typical networks.

At low-circuit loads, the overestimation at downstream links of the tandem network increases. This is because, at downstream links, there is proportionately more internodal bursty packet traffic than fresh Poisson packet traffic. Thus, at low and medium circuit loads, the further downstream a link is, the more is the effect discussed in the previous paragraph (note that the tandem network is symmetric with respect to circuit traffic). At high-circuit loads, there are mostly single link circuits and hence the approximation underestimates at all links.

5. Networks with multiple channels per link

We also apply the approximate analysis to networks with multiple channels per link. We used the approximation procedure (outlined in Kelly[3]) to calculate blocking probabilities of various links in a 6-node tandem network in which each link has four full duplex channels, three dedicated to circuit-switched traffic and one to packet-switched traffic. We approximate each link of the network by an isolated link with the same number of circuit channels and packet channels and a Poisson circuit arrival process and a Poisson packet arrival process. Assuming that the link-blocking probability calculated by the fixed point method[3] is due to a Poisson circuit arrival process, we calculate the equivalent Poisson circuit arrival rate, using Erlang's formula. Further, given the packet arrival rate for each source-destination pair, and the routing matrix, we find the packet arrival rate at each link. This yields an approximate model for each link, whose analysis we have basically adopted from Kraimeche and Schwartz[6].

By comparing mean delay experienced by packets obtained through simulation at link 3 of a 6-node tandem network with each link having four full duplex channels, three dedicated to circuit traffic and one to packet traffic and their corresponding approximate estimates, we make the following observations.

In the underload region, packets do not rely much on circuit channels. Hence, the approximation technique works well. In fact, if there were no circuits at all, the packet network would be product form and the analysis would be exact. Near overload region, the positive correlation between server availability

and arrival of bursts to the server is not much, because again packets do not rely that much on circuit channels, when the circuit occupancy is low. But, as circuit occupancy increases, this correlation decreases and arriving bursts experience more delay. Hence, the approximation works well at low-circuit occupancies and underestimates at high-circuit occupancies. In the deep overload region, there exists a very good positive correlation between server availability and arrival of bursts to the server, when the circuit occupancy is low and hence approximation overestimates. As circuit occupancy increases, because of decrease in this correlation, the approximation underestimates.

6. Adaptive routing of packet traffic

If alternate routing is possible for packets then we can adaptively route the packets to improve the performance of packets in an integrated services network. We study only the case of a single channel per link. Circuit traffic follows fixed routing.

In the first adaptive routing technique, selection of one, among various alternate links, which can reduce the number of hops to reach the destination by one, is done based on mean work at these links. We also consider a variant of this technique. In this case, the selection is done by considering the length of multiple link circuits on these alternate links in addition to considering the mean work at these links.

We implemented both the above techniques in the simulation of a d2 hypercube network. Both the adaptive routing schemes are based on the mean work at any queue which is obtained essentially from our approximate model. Comparing simulation results those based on adaptive routing with the simulation results that are based on usual routing, we conclude, that the adaptive routing based on mean work is more effective as the packet load increases and is less effective as the circuit load increases. This is because the fluctuation of packet traffic is much more as packet load increases compared to that caused by increase in circuit load. Our variant adaptive routing technique also behaves in the same way except that it improves the delay performance of packets slightly at low circuit load compared to the adaptive routing technique that is based on mean work.

References

1. FISCHER, M. J. AND HARRIS, T. C. — A model for evaluating the performance of an integrated circuit- and packet-switched multiplex structure, *IEEE Trans.*, 1976, **Com-24**, 195–202.
2. BURMAN, D. Y., LEHOCZKY, J. P AND LIM, Y. — Insensitivity of blocking probabilities in a circuit-switching network. *J. Appl. Probab* , 1984, **21**, 850–859.
3. KELLEY, F. P. — Blocking probabilities in large circuit-switched networks, *Adv. Appl. Probab.*, 1986, **18**, 473–505.
4. LAVENBERG, S S. — *Computer performance modelling handbook*, 1983, Academic Press
5. BURKE, P. J. — Output of a queueing system, *J. Op Res. Soc. Am.*, 1956, **4**, 699–704.
6. KRAIMECHE, B. AND SCHWARTZ, M. — Analysis of traffic access control strategies in integrated services networks. *IEEE Trans.*, 1985, **Com-33**, 1085–1093.

Thesis Abstract (M.Sc. (Engng))

Self-synchronization of step motor using current difference method by K. Muthukumar
Research supervisor: N. J. Rao
Department: Computer Science and Automation

1. Introduction

Precision motion control systems are required in a large number of applications like biomedical and analytical instruments, computer peripherals, machine tools, robots, automobiles and all types of manufacturing equipment. These systems may be built around electromechanical, hydraulic or pneumatic actuators. Some

of the commonly used electromechanical actuators are step motors, dc and ac servo motors and solenoids. One of the most popular electromechanical actuator used is the step motor. The step motor is an electromagnetic device which converts digital pulse inputs into incremental output motion. Each pulse advances the step motor by a step increment and latches it magnetically at the precise point to which it is stepped. It is this precise stepping characteristic that makes step motor most attractive, as it can be operated, in principle, in an open-loop mode.

The open-loop mode of operation for step motor is simple and inexpensive. It consists of switching the supply to various phases of the motor winding in a sequential manner at predefined time intervals. Each switching will make the rotor to move by a fixed angular increment, without any risk of cumulative angular error, as long as the load and acceleration/deceleration rates remain within acceptable range.

In open-loop mode of operation, the motor cannot be operated at any speed where the load torque is equal to the motor dynamic torque, which will lead to loss of synchronism. To avoid this loss of synchronism, some safety margin should be given between the load torque and the motor torque throughout the speed range. This safety margin leads to under utilisation of torque capabilities of the motor. The performance of a step motor can be greatly enhanced if it is operated in closed-loop, using some form of self-synchronisation[1].

In self-synchronisation, the phase voltages are switched with reference to the rotor position. The motor phase current lags from the voltage depending on the motor speed because of the inductive behaviour of the motor winding. For an optimum motor torque the phase angle between the supply voltage and the rotor position should be varied depending on the motor speed to compensate the lag in the phase current[2]. The rotor position can be derived directly with an encoder coupled to the rotor. However, the use of encoder increases the inertia, space requirement and cost. To overcome this, many indirect methods of deriving the position information have been developed. Most of these methods have difficulties at the implementation level.

2. Current difference method[3]

A new method has been developed to derive the rotor position indirectly, termed as current difference method. The current difference is the difference between the actual current in one phase of the motor and the corresponding current that would circulate in the same phase in a stalled motor. In actual case, the stalled motor current is simulated with an RC circuit whose time constant is matched to the motor electrical time constant. The actual phase current is measured with a current shunt. This current difference signal is the current that would circulate in a phase due to back EMF only.

This current difference signal is used as reference to switch the phase voltages. The signal is a sinusoidal waveform, which is converted into a square waveform and directly used to switch the motor voltages. This waveform is to be delayed depending on the motor speed for an optimum motor torque generation. A closed-loop step motor system was simulated to establish the effectiveness of the proposed self-synchronisation scheme. Based on the simulation results a microprocessor-based controller was designed. The values of the delay that needs to be introduced were stored as look-up tables. The speed of the motor is derived by measuring the current difference waveform pulse width. The pulse width data is used as pointer to fetch the delay data from the look-up table. This delay data is loaded into digital monostable which delays the switching voltage. With this controller, the motor is made to generate optimum torque throughout the speed range. Practical results have shown good correlation with simulated data.

3. Practical implementation[4]

A point-to-point positioning system with indirect rotor position sensing was designed. This system was based on an 8-bit microprocessor. In this point-to-point move, the controller starts the motor a few steps in open loop and switches to self-synchronisation. This open-loop start is required because the current difference signal for switching the phase voltage will not be available when the rotor is stationary. Once the motor is switched into self-synchronised mode, the motor goes into acceleration phase and the speed increases to a maximum value where the motor dynamic torque matches the load torque. Since the motor rotates in self-synchronised mode, it will continue to rotate even when the motor torque is equal to load torque, which is not the case in open-loop operation. The controller has to keep some steps for deceleration from the total steps to be moved. The number of steps reserved for deceleration is taken as multiples

of the number of steps taken by the motor during the acceleration phase. In short moves, the motor will not reach the maximum speed because the controller will start the deceleration phase before it reaches the maximum speed

The deceleration is the difficult phase in a move, where the motor should stop without any over shoot. The method of deceleration tried here is simple and gives good results. The delay data which was used during the acceleration phase is loaded into the digital monostable in a reverse order after the motor moves through a multiple of the step. This type of acceleration and deceleration mode can take some amount of load variation, as proven by experimentation.

4. Effect of parameter variation[5]

The circuitry used to derive the current difference signal is very simple to implement, in comparison to other methods reported in literature. With minor modifications this circuit has been adopted to chopper drives as well. But in any of these methods of indirect measurement of the rotor position using passive elements, it is necessary to establish the validity of the signal under all operating conditions, as the parameters of the circuit can only be perfectly matched with those of the motor at any one operating point. The parameters of the motor will change with temperature or from motor to motor of the same name plate ratings. It is established both theoretically and experimentally that the effect of parameter variation is insignificant on the behaviour of the closed-loop system.

5. Conclusions

Operating the step motor under self-synchronised mode based on the current difference method leads to good dynamic performance and makes the system less sensitive to parameter variations. The deceleration method tried was not efficient and requires further study. All the techniques developed through this study can also be implemented for brushless dc motors.

References

1. KUO, B. C. — *Closed loop and speed control of step motors*, 1974, IMCSS, Champaign.
2. ANTOGNINI, L — *Dynamic torque optimization of a step motor by back EMF sensing*. 1985, IMCSS, Champaign.
3. PITTET, A AND MUTHUKUMAR, K. — *Step motor performance optimisation by closed loop control using the current difference method*, 1988, IMCSS, Champaign.
4. MUTHUKUMAR, K., PITTET, A. AND RAO, N.J. — *Implementation of a closed loop control technique for a point-to-point positioning system using step motor*, 1988, IMCSS, Champaign
5. MUTHUKUMAR, K., PITTET, A. AND GERBER, G — *Effect of parameter variation on self-synchronisation scheme using step motor*. 1990, IMCSS, Champaign.

Thesis Abstract (M.Sc. (Engng))

Bending analysis of truncated conical shells by Meghal S. Karekar
Research supervisor: K. Chandrashekara
Department: Civil Engineering

1. Introduction

Closed truncated conical shells are widely used in civil engineering practice as chimney stacks, shafts of elevated water tanks and for foundations of tall structures. These structures are generally subjected to asymmetric loads like wind load, soil reaction, etc. Open conical shells have wide application as roofing elements and are normally subjected to dead and live loads. This work attempts to provide a practical insight to the behaviour of closed conical shell subjected to asymmetric load and conical shell panel subjected to dead load.

2. Method of analysis and results

A simplified set of differential equations, similar to Donnell's equations for cylindrical shell, have been used to study the bending behaviour of truncated conical shell of revolution and panel of constant thickness. The governing partial differential equations have been reduced to ordinary differential equations, in axial coordinate, by using Fourier series expansion in the circumferential direction. These ordinary differential equations will have variable coefficient and have been solved by using finite difference method[1]. Numerical results have been obtained for two sets of boundary conditions for a truncated conical shell of revolution, namely, larger end fixed and smaller end free and *vice versa*. As a limiting case, results for a cantilever cylindrical shell of revolution subjected to wind load have been obtained and a comparison with the available results has been made. For a cantilever truncated conical shell of revolution results have also been obtained by using the power series method[2] and these have been compared with the results obtained using the finite difference method. Some of the results of bending analysis have also been compared with the membrane theory results.

Analysis of an allround simply supported conical shell panel subjected to either dead load or a cosine load variation has been made by using Fourier expansion in transverse direction which satisfies the simply supported boundary. An experimental study using the photoelastic method has also been made for a conical shell panel subjected to a cosine load variation. Stress freezing and slicing techniques have been used to find the stress distribution along some sections of the shell and have been compared with the results of the numerical method.

3. Conclusions

It has been shown that the numerical method adopted here is computationally more efficient compared to the power series method. It is also shown that for conical shells of revolution with base angle greater than 75°, the membrane theory is valid over the major portion of the shell (except near the fixed edge). For purpose of design, an equivalent cylindrical shell analysis concept has been introduced particularly to determine the longitudinal bending moment in the shell. Experimental results confirmed the accuracy and reliability of the results obtained from the numerical method.

References

1. BUDIANSKY, B. AND RADKOWSKI, P.P. Numerical analysis of unsymmetrical bending of shells of revolution, *AIAA J.*, 1963, **1**, 1833–1842.

2. WILSON, B. Asymmetrical bending of conical shells, *J. Engng, Mech. Div., Proc. ASCE*, 1960, **86** (EM3), 119–139.

Thesis Abstract (M.Sc. (Engng))

Dynamic analysis and random process modelling of railway tracks by O. R. Jaiswal
Research supervisor: R. N. Iyengar
Department: Civil Engineering

1. Introduction

Proper understanding of dynamic behaviour of railway tracks is essential to provide fast, efficient and safe transportation. The main function of a railway track is to safely distribute the weight of the train to the ground. Thus, railway track acts as a load-carrying structural system which provides elastic support to the moving loads. However, in the process, with the passage of time the track settles at points of high stresses. This leads to the development of irregularities in the track in various directions. It is necessary to measure and model these irregularities systematically so as to properly understand the track dynamics and to

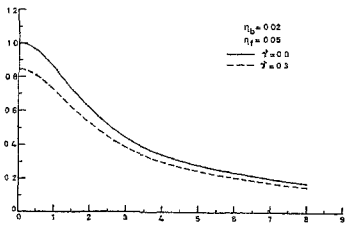

FIG. 1. Effect of foundation inertia on the critical velocity

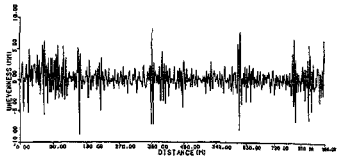

FIG. 2 Vertical uneveness record.

:haracterize the random dynamic forces acting on the vehicles. Thus, structural properties and geometrical ›roperties are of prime importance in characterizing railway tracks.

?. Scope of the present work

The work reported aims at understanding the influence of track–foundation interaction and track ir-'egularities on the dynamic behaviour of railway tracks. The scope of the investigation is as follows:

1) To develop a generalised beam on elastic foundation (BEF) model for railway tracks, which can include the effect of foundation inertia.
2) To develop a random process model for track unevenness from measured data.

3. Summary, results and discussion

3.1. *Structural model for railway track*

The most popular model for the analysis of railway treks under a moving force is the BEF model[1], consisting of an infinitely long beam resting on a set of closely spaced independent springs. However, this model does not account for the foundation inertia, which considerably influences the response under dynamic conditions[2]. In the present investigation, the effect of foundation inertia is included by modelling the track as an infinitely long beam resting on a series of closely spaced, independent axial rods of finite length, fixed at the bottom and connected to the beam at the top. The effect of an axial thrust in the beam is also included along with the effect of damping in the beam and foundation. The foundation inertia has been shown to be important in as much as it can reduce the critical velocity significantly. Also, the foundation inertia can induce higher stresses in the foundation leading to separation between the beam and the foundation. In Fig. 1, the effect of foundation inertia on the critical velocity is shown. In this figure, α_{cr} is the critical velocity parameter and β, the mass parameter. $\beta = 0$ corresponds to the massless foundation case. The effect of axial force parameter is also depicted in this figure.

3.2. *Modelling of vertical track irregularity*

Recorded data of vertical unevenness and absolute vertical profile (AVP) from various stretches of Indian railway tracks have been statistically analysed. A record of vertical unevenness over a kilometer length is shown in Fig. 2. A stationary gaussian random process model is proposed for the vertical irregularity. Such a process is completely defined by its PSD function. Two typical PSD functions are shown in Fig. 3. As a practical application of the model, a theoretical estimate of the peak amplitude of various orders in a given track length is obtained. Numerical results from this estimate are compared with actually observed values to validate the proposed model. The comparison is found to be good. Results of such a comparison for two different track stretches are shown in Table I. Here ε is a parameter estimated from the PSD function. L_d is the length of the track stretch. N is the total expected number of peaks and α is the peak amplitude standardised with respect to the standard deviation.

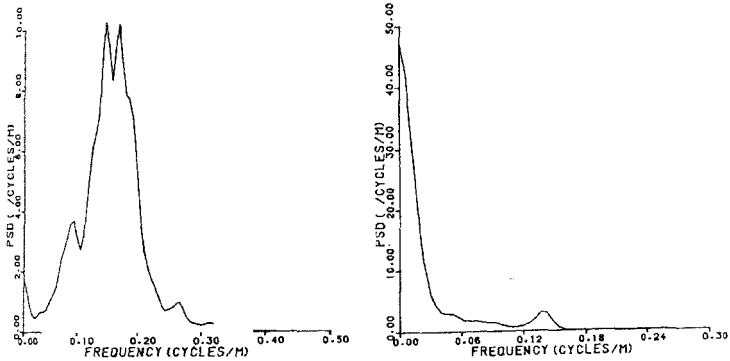

FIG. 3. PSD functions for (a) vertical unevenness and (b) AVP.

Table I

Peak amplitudes

S1IL, ϵ = 0·548, L_d = 900 m, N = 174

Order j	1	2	3	4	5	6	7	8	9	10
Estimated (α)	4·377	3·709	3·406	3·214	3·073	2·962	2·870	2·792	2·724	2·663
Observed (α)	4·136	3·930	3·638	3·346	3·055	2·972	2·890	2·807	2·725	2·643
S3IL, ϵ = 0·925, L_d = 880 m, N = 110										
Order j	1	2	3	4	5	6	7	8	9	10
Estimated (α)	4·089	3·363	3·028	2·813	2·653	2·526	2·419	2·328	2·247	2·175
Observed (α)	3·400	3·009	2·963	2·854	2·834	2·189	2·142	2·094	2·056	1·982

Possible improvements to the track model in the light of the above studies have also been discussed. In particular, equations of motion which can include the random vertical profile of the track and inelastic foundation behaviour are derived.

4. Conclusions

The study reported here contributes to a better understanding of track–foundation interaction and track irregularities. The results can be directly used for finding the critical velocity of a track which is an important design parameter. From the knowledge of an estimated PSD function, for track irregularity, the number and level of the peaks can be found by the procedure explained in the thesis.

References

1. KERR, A. D. The continuously supported rail subjected to an axial force and a moving load, *Int. J. Mech. Sci.*, 1972, **14**, 71–78.

2. HOLDER, B. W. AND MICHALOPOULOS, C. D. Response of a beam on an inertial foundation to a travelling load, *AIAA J.*, 1977, **15**, 1111–1115.

hesis Abstract (M.Sc. (Engng))

PC-based interferometer for radio astronomy by N. Jayaprakash

esearch supervisors: B. S. Sonde and V. Radhakrishnan (Raman Research Institute)
epartment: Electrical Communication Engineering

. Introduction

terferometry is now a well-established experimental technique of considerable importance in science and chnology. In these nearly ten decades of its existence, it has advanced greatly, almost in step with the dvances in electronics, optics and related fields. While the first interferometer was developed by Michelon in 1890 to estimate stellar diameters, more recent developments in interferometry have taken its pplication areas into other branches of science, such as radio astronomy, spectroscopy, etc. To the astonomer, interferometry provides a means of measurement of stellar diameters and more recently a powerful tool in high-resolution radio astronomy, both implying studies of the angular distribution of radiation n the sky. For the spectroscopist, it facilitates measurement of spectral distributions and represents a new chnique for high-resolving power and increased sensitivity. To the optical designer, it is a method of sting lenses and, to the biologist it is a new branch of microscopy. To the metrologist and the engineer, is now an important means of converting the international standard of length into a practical scale.

Interference occurs when radiation follows more than one path from its source to the point of detection. may be described as the departure of the resultant intensity from the laws of addition. This is because s the point of detection is moved, the intensity oscillates about the sum of the separate intensities from ch path, leading to maxima and minima in the intensity pattern. These are generally called interference inges. The technique of interferometry is derived from these interference patterns. And today, it has volved into one of the most important methods of experimental physics, with applications extending to any branches of science and technology, as indicated earlier.

The first use of interferometry in radio astronomy was reported in 1947[1,2]. Since then, many radio terferometers have been developed and used in astronomical studies[3,6]. The first radio interferometer ade use of the reflections from the surface of the sea to provide the second path; but later instruments ere developed making use of two separate antennas in the system. The powerful technique of aperture nthesis was a spin-off from radio interferometers. This technique has formed the basis for several new dio telescopes that were built in later years, with resolutions, until then thought of as unrealisable. Some these interferometers are now operating over a wide range of radio frequencies for a variety of astonomical applications all over the world. In the last over four decades, there has been considerable velopment and improvement in the techniques employed, and the electronics involved in realising these terferometers. Major advances in interferometry in recent years have largely been influenced by:

a) Progress in electronics,
b) Advances in computers; and
c) Wider range of applications.

While the advances in electronics during this period have greatly influenced the development of better d improved instrumentation for the radio interferometer, progress in digital computers has contributed great deal in the field of analysis of observed data. This is particularly important as the study of the stribution of radiation over the sky involves manipulation of a large database. However, more recently, the cost of computers has begun to decrease and their functionality increased, they have also been used r data acquisition in radio interferometry. As a result, there is now a wide variety of mainframe and inicomputers in use all over the world in radio astronomy applications. However, some limitations are ffered by these radio interferometer systems. A few of them are:

a) Lack of standardisation in data structures
b) Incompatibility of secondary storage media
c) Multiplicity of programs for the same type of analysis in different systems
d) Need for two separate computers, *viz.*, (i) data acquisition, and (ii) data analysis.

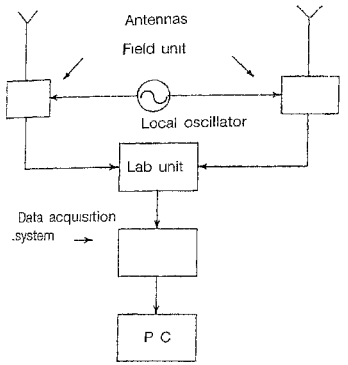

FIG. 1 Radio interferometer.

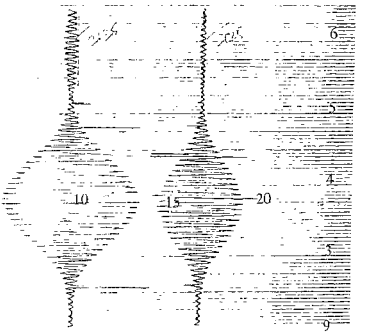

FIG. 2. Cygnus A (3C 405)-Interferometer fringes.

This has resulted in the data acquired at one location not being easily analysed at another location leading to problems in free exchange of unprocessed data from one observatory to another. This has also resulted in lack of flexibility that is so much needed in this important field. Also there is a need for preliminary online data analysis, to monitor it for interference, which is especially predominant at low frequencies. This would avoid the collection of unnecessary data, thereby saving data storage space. Considering these limitations, and keeping in view the recent developments in personal computers (PCs) and their possible uses in instrumentation, it was decided to conduct a detailed investigation on the use of PCs to radio interferometer at 150MHz, it was decided to try out the new ideas resulting from this investigation in the system design and implementation of this new interferometer. This interferometer, which can be aptly termed as an intelligent instrument, would not only solve the problem of data transportability but also incorporate a real-time data acquisition system (DAS) in it. This would enable online data acquisition, interference monitoring and storage, as well as offline data analysis all in the same system. The result of this investigation is the development of a PC-based radio interferometer, which is described in detail.

2. Highlights and results

The highlights of the work are the development of a PC-based radio interferometer with the following important characteristics:

a) Standardisation in data structure
b) Flexibility of data manipulation online
c) Easy transportability of unprocessed data between different observatories
d) Facilty for real-time interference rejection
e) Convenient initial data processing offline
f) Low cost in system implementation.

The main contributions of the work are:

a) A detailed analytical study of a DAS
b) Design and development of a PC-based DAS
c) Experimental verification of the DAS by simulation
d) Overall system integration to realise a PC-based radio interferometer (Fig.1)
e) Conducting initial astronomical observations using this system.

The fringes obtained from a radio source (Cygnus A) using this interferometer are shown in Fig. 2. The number of fringes expected for this source and that actually measured by the system tally fully, clearly indicating satisfactory overall performance.

3. Conclusions

These studies and investigations have indicated that a PC-based system is attractive in several respects for a small radio interferometer. The preliminary tests conducted so far on astronomical observations, show that this interferometer can give useful data/results in an economical and elegant manner. Considering the present trends in PCs, *i.e.*, availability of more and more computing power at higher and higher speeds at steadily decreasing costs, it is likely that this approach will become more popular and an accepted standard practice in future instrumentation for radio astronomical applications of similar scale.

References

1. KRAUS, J D. — *Radio astronomy*, 2 edn, 1988, McGraw-Hill.
2. CHRISTIANSEN, W. N. AND HOGBOM, J. A — *Radio telescopes*, 2 edn, 1985, Cambridge Univ. Press.
3. STEEL, W. H. — *Interferometry*, 1967, Cambridge Univ. Press.
4. HADDOCK, F. T. — *Proc. IRE*, 1958, **46**, 3–12
5. KALACHOV, P. D — *Proc. IRE, Aust*, 1963, **24**, 237–242
6. HILLS, R E. *et al* — *Proc. IEEE*, 1973, **61**, 1278–1282

Thesis Abstract (M.Sc.(Engng))

Analysis of tropical convection using satellite data by Asha Guruprasad

Research supervisor: Sulochana Gadgil
Department: Centre for Atmospheric Sciences

1. Introduction

Organised convection in the tropics occurs primarily in the intertropical convergence zone (ITCZ). Many of the important phenomena in the tropics such as the El-Nino or the monsoons involve large displacements of the ITCZ. Understanding the nature of the space-time variations of the ITCZ is therefore an important problem in tropical meteorology. After the advent of meteorological satellites, it has become possible to study the variation of the planetary scale convection over time scales ranging from the daily to interannual by analysis of the relevant fields such as the outgoing longwave radiation (OLR), albedo (reflectivity of the radiating surface), etc. The work reported is aimed at increasing our knowledge of the nature of the intraseasonal and interannual variations of the ITCZ using digital satellite data.

The monsoon is a manifestation of the migration of the ITCZ from the oceanic region on to the Indian subcontinent during the summer season. Major features of the intraseasonal variations of the ITCZ over the Indian longitudes during the summer monsoon have been brought out by earlier studies of satellite imagery. These are:

(i) Oscillations in the intensity of the continental ITCZ between active and weak spells or breaks.

(ii) A bimodal distribution of convection with latitude due to the presence of an ITCZ over the equatorial Indian Ocean as well as one over the continent.

(iii) Poleward propagations of the ITCZ from the equatorial Indian Ocean on to the continent at intervals of 2-6 weeks.

2. Contributions of the thesis

In order to study whether these features are observed over other parts of the tropics, an objective method

to delineate the ITCA from the $2{\cdot}5^0$ daily data on OLR and albedo has been developed[1]. The method involves identification of the grid points with a large fraction of deep convective clouds by the imposition of a bispectral threshold (185 WM^{-2} for daytime OLR and 0·5 for albedo). Such selected grid points are then filtered to retain only the large-scale convection. The variations of the ITCZ deduced by this method compares well with that obtained by the subjective analysis of satellite imagery[2]. The region of convection delineated is very similar to that obtained by the analysis of the equivalent blackbody temperature data on pixel scale[3].

2.1. *Analysis of the interannual variation*

The intraseasonal variation of the ITCZ over different parts of the tropics is analysed. It is found that oscillation between active and weak spells is a basic feature of the ITCZ. Bimodality is found only over the Asian monsoon zone. Poleward propagations are seen over the Asian winter monsoon regions only in some years.

2.2. *Analysis of the interannual variation*

The interannual variation of the ITCZ has been studied. Since rainfall is known to be well correlated with the presence of highly reflective clouds in the tropics[4] we expected the variation in the number of convective days in a month (counted as the number of days on which the threshold criteria for OLR and albedo are satisfied) to be related to the variation in the rainfall over the Indian region. However, the interannual variation of the number of convective days during the period 1974–1985 was found to be not completely consistent with that of rainfall. Therefore, the variations of a more basic variable, *viz.*, monthly mean OLR were analysed. This analysis of the variation of the OLR and rainfall over the Indian region suggests the possibility of a systematic bias in the OLR (both daytime as well as daily average) with consistently lower values during 1982–85 as compared with 1974–78. It is also shown that the bias can be removed by an empirical formula akin to the one used in earlier corrections[5].

References

1. GADGIL, S. AND GURUPRASAD, A. — An objective method for the identification of the intertropical convergence zone, *J Climate*, 1990, **3**, 558–567.
2. SEKA, D. R AND GADGIL, S. — On the maximum cloud zone and the ITCZ over the Indian longitudes during the southwest monsoon, *Mon Wea Rev.*, 1980, **108**, 1840–1853.
3. MURAKAMI, M. — Analysis of the deep convective activity over the western Pacific and southeast Asia, Part I: Diurnal variation, *J. Met. Soc. Jap.*, 1983, **61**, 60–76.
4. KILONSKY, B. J. AND RAMAGE, C. S — A technique for estimating tropical ocean rainfall from satellite observations, *J. Appl. Met.*, 1976, **15**, 972–975.
5. GADGIL, S., GURUPRASAD, A. AND SRINIVASAN, J. — Systematic bias in the NOAA outgoing longwave radiation data set, *J. Climate*, 1992, **5**, 867–875.

Thesis Abstract (Ph.D.)

Modelling the lifted minimum phenomenon in the atmosphere by A. S. Vasudeva Murthy

Research supervisors: R. Narasimha, J. Srinivasan and S. Kesavan (TIFR)

Department: Mechanical Engineering

1. Introduction

The Ramdas paradox or the lifted minimum phenomenon has been a long-standing micrometeorological puzzle. It concerns the vertical distribution of air temperature which, near the ground during nights, shows, in general, increase with height up to some distance above the ground before it starts falling. However, Ramdas and Atmanathan[1] reported that on calm clear nights in Pune and other places in India

they observed the minimum temperature not at the ground but at a height of order 20 cm (Fig. 1) abo it. These observations are intriguing because ground (with infrared emissivity close to one) is a go radiator compared to air (less than 0·3) and hence may be expected to cool to a temperature below th of air above it. Ramdas and Atmanathan found that the layer of air at 20 cm remained cooler than t ground for well over three hours. Although these results were at first treated with suspicion, they ha since been amply confirmed by many other investigators in different parts of the world (Lake[2]), leadi to what has since become known as the lifted minimum phenomenon or Ramdas paradox. Raschke[3] a Oke[4] have made exhaustive and well-documented studies. Oke, in particular, states that clear skies a 'winds below 1m/s (at a height of 25 cm) appear to be the two basic requirements for the existence of t lifted minimum.

Several physical explanations of the phenomenon have been offered, in particular by Ramanathan a Ramdas[5], Lake[6] and Geiger[1]. Although most investigators consider radiation to play a dominant role i the occurrence of the lifted minimum, the different explanations are generally contradictory and the preci mechanism has never been quantitatively explained.

The only attempt so far at a mathematical treatment of the problem is due to Zdunkowski[8], whos numerical calculations assuming a quasi-gray radiative model indicated that the existence of a haze laye near the ground is essential for the occurrence of the lifted minimum. There are two main difficulties wit this model. Firstly, no haze layer was reported by either Ramanathan and Ramdas[5] or Oke[4]. In particula Oke (being aware of Zdunkowski's theory) was specially looking for possible haze. Secondly, the therm diffusivity assumed by Zdunkowski at heights below 10 cm is about 18 times lower than the molecul value for air, which is unphysical

2. Model description

The present work attempts to explain the phenomenon by formulating and solving the appropriate energ transport equation under the conditions that appear necessary to cause the lifted minimum. It is assume that (1) surface temperature variation, atmospheric humidity and wind can all be considered to be pre scribed; (2) there is no atmospheric scattering: and (3) the temperature T is homogeneous in the horizonta plane, and so depends only on height z and time t. The evolution of the temperature profile is the governed by energy balance,

$$\rho_a c_p \frac{\partial T}{\partial t} = -\frac{\partial}{\partial z}(Q_c + Q_t + Q_r) \tag{1}$$

where ρ_a is the density of air, c_p, the specific heat of air at constant pressure, and the total energy flu is conveniently split into conduction (Q_c), convection (Q_t including turbulent transport) and radiation (Q_r) Q_t is assumed to be porportional to the gradient of the potential temperature through an eddy diffusivit that is itself proportional to the friction velocity u^* times z and a function of the Richardson number tha is derived from the extensive experimental data avaiable. A simple broadband flux emissivity model i used for Q_r. The resulting nonlinear partial integro-differential equation is then supplemented with th following initial/boundary conditions. At the lower boundary (taken as ground) the temperature at time after sunset is prescribed as

$$T_g(t) = T_{go} - \beta \sqrt{t}\,, \tag{2}$$

where β is a constant that varies with the inverse square root of the thermal conductivity of the soil. As $z \to \infty$ the temperature is assumed to fall at the standard lapse rate (Γ) of 9·8 K/km

$$\frac{\partial T}{\partial z}(z \to \infty,\ t) = -\Gamma\,.$$

The initial condition is prescribed to be

$$T(z,o) = T_{go} - \Gamma z\,. \tag{4}$$

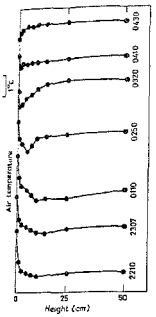

FIG. 1 Nocturnal evolution of temperature profiles showing a lifted minimum at Hamilton, Canada, on 1-2 July 1966

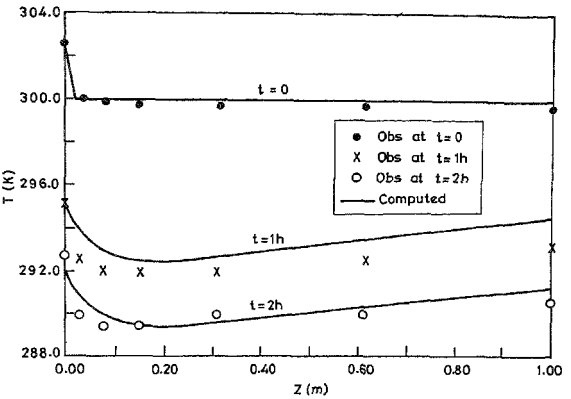

FIG 2. Comparison of computed and observed temperature profiles with a lifted minimum.

The resulting initial/boundary value problem is then solved by the method of lines with a spatial discretization that allows for a progressively finer resolution as the surface is approached.

3. Results and conclusions

As noted above most investigators have suggested that radiation plays a strong role in the formation of the lifted minimum. Therefore, in the first instance, heat transfer due to radiation alone was considered in eqn (1), *i.e.*, we set $Q_c \equiv Q_t \equiv 0$. The resulting equation was then integrated up to two hours. The solutions obtained show the classical radiative slip (or discontinuity) at the ground. The slip $[T_g(t) - T(0^+,t)]$ is then studied as a function of ground emissivity (ϵ_g), ground cooling rate (β) and humidity content (q_0) near the ground. It is then shown that the slip varies rapidly with ϵ_g and β. In particular, for values of ϵ_g not too close to unity ($< 0{\cdot}994$) and β not too high ($< 7\ \mathrm{K}/\sqrt{\mathrm{h}}$) the temperature profiles show a strong resemblance to the observations with lifted minimum. However, these profiles are characterized by discontinuities and have the air layer just above the ground ($z = 0^+$) as the level of minimum temperature. This leads to the surmise that the lifted minimum could be caused by the smoothing of the radiative slip by thermal diffusion (molecular, turbulent or both). Consequently, Q_c and Q_t are introduced in succession and the resulting equation is again integrated for up to two hours. The solutions obtained by introducing Q_c show a lifted minimum at heights varying between 15 and 30 cm. The solutions obtained by introducing Q_t tend to weaken the structure of the lifted minimum. By further computations, it is shown that the amount of Q_t at 25 cm should not exceed about four times that of Q_c if a lifted minimum is to form. In the next instance, the temperature profile of air near the ground just after sunset and the observed ground cooling taken from Ramanathan and Ramdas[5] are used as initial and boundary conditions on eqn (1) and the solutions are compared with observations. Good agreement is found between the calculated and the observed temperature profiles (Fig. 2). The dependence of the lifted minimum on the parameters ϵ_g, β and q_0 is then studied, leading to maps which should be useful in predicting the phenomenon. In addition, the lifted minimum as a function of the surface Boltzmann number (ratio of convective energy flux to that of radiative energy flux) and other associated nondimensional numbers is also studied.

References

1. RAMDAS, L. A. AND ATMANATHAN, S *Beit. Zur. Geophys.*, 1932, **37**, 116–117.
2 LAKE, J. V. *Nature*, 1955, **176**, 32–33.

3.	RASCHKE, K.	*Met Rundsch.*, 1957, **10**, 1–11.
4.	OKE, T. R	*Q. J. R. Met. Soc*, 1970, **96**, 14–23
5.	RAMANATHAN, K. R. AND RAMDAS, L. A.	*Proc. Indian Acad Sci*, 1935, 1. 822–829
6	LAKE, J. V.	*Q. J Met. Soc.*, 1956, **82**, 187–197.
7.	GEIGER, R.	*The climate near the ground*, 1965, Harvard University Press
8	ZDUNKOWSKI, W.	*Beitr Phys Atmos.*, 1966, **39**, 247–253.

Thesis Abstract (M.Sc.(Engng))

Sparkover characteristics of inhomogeneous field gaps in compressed SF_6 under composite stresses by G. S. Punekar
Research supervisor: M. S. Naidu
Department: High Voltage Engineering

1. Introduction

Although electrical characteristics of SF_6 have been extensively studied for both uniform and non-uniform field conditions with ac, dc and impulse voltages, relatively very little work has been done using composite voltage (impulse voltage superimposed on dc or ac voltage) stresses, especially under non-uniform fields. Studies with impulse voltages superimposed on dc are important due to the following reasons[1,2]:

a) In a dc–GIS, these are the typical voltages encountered.
b) The disconnector switch of the Ac–GIS also experiences these stresses under practical conditions, and
c) The composite voltage studies with inhomogeneous fields help in a better understanding of corona stabilization and its influence on the breakdown of electronegative gases.

In a practical system, the fault initiation is always from a point of inhomogeneity which may be in the form of a microprotrusion or a fine metallic particle and these cannot be avoided for sure[3].

In view of the above, composite voltage characteristics of SF_6 gas gaps were investigated in detail along with pure dc and lightning impulse voltage characteristics. The investigation was carried out using the needle plane and hemispherically capped rod-plane gap configurations with two different field factors, (f = 9·744 and 24·93, respectively), for a 10-mm gap separation, over the SF_6 gas pressure range of 0·1 to 0·5 MPa (absolute). To facilitate the experimental work, a high-pressure test chamber along with an inexpensive SF_6 recycling system was specially designed, fabricated and tested to meet the scarcity and cost considerations of the SF_6 gas.

The circuit arrangement used to produce composite voltages is shown in Fig. 1. The results reported here are for the laboratory pure (99·8%) SF_6 gas gaps. No external irradiation of the gap was employed in the present investigation. The voltage-pressure characteristics of the needle plane gap with pure dc and standard lighting impulse (1·2/50 us) stresses are as shown in Fig. 2. The experimental results of the first quadrant and the fourth quadrant study (rod-plane gap) are given in Fig. 3. The mean values indicated in these figures are the 50% probability breakdown voltages (V_{50}) obtained using the 'up and down' method (a statistical technique). Also marked on the X-axis are the positive dc corona inception voltages. The overall accuracy of the V_{50} values is better than ± 5%.

2. Results and discussion

From Fig. 2, comparing the positive dc breakdown voltages with the positive impulse voltages over the pressure range studied, it is seen that the anamolous behaviour of the gas results in impulse ratio less than one. This strange behaviour is being widely studied[4] and is thought to be due to space charges in

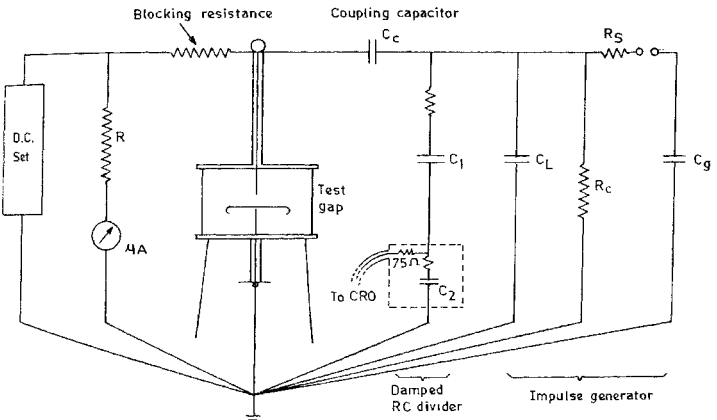

Fig 1. Circuit for dc-bias studies.

the gap prior to sparkover. In this region, termed as the corona stabilization region, sparks curved in shape were observed due to the neutralisation of the positive ion space charge which results in the weakening of the electric field along the gap axis (see Fig.4).

From the first quadrant study (Fig. 3) for dc bias voltages below the corona onset voltage, an increase in the total (composite) breakdown voltage is observed when compared to the pure impulse breakdown voltage (without the dc bias). A similar observation was made earlier by Gockenbach[1] for the case of a 25-mm dia sphere to plane gap of 3 mm, at a pressure of 0·1 MPa. Increase in the dc bias voltages above the corona onset voltage was observed to increase the total breakdown voltage which is attributed to the space charge shielding around the point electrode. It is also observed that the breakdown voltages obtained with the composite voltages are always higher than those obtained at either the lightning impulse voltage or the dc voltage acting separately. A similar observation for the switching impulse voltage superimposed on the ac peak was also reported by Anis and Srivatsava[5].

For the unlike polarity composite voltages (4th quadrant) a decrease in the total breakdown voltage with the increase in the dc-to-impulse ratio is observed. The most important observation to be made is that the breakdown voltages obtained with the composite voltages of this type can be lower than either the dc voltage or the lightning impulse voltage acting separately at this gas pressure, *i.e.*, 0·2 MPa (near the most effective corona stabilization region)

3. Conclusions

The study has led to a better understanding of the anamolous behaviour of SF_6 which is due to space charges. Also, the criticality of the composite stresses (of polarity reversal type) in deciding the withstand levels of non-uniform SF_6 configuration has been brought out.

References

1. Gockenbach, E. Influence of pre-existing dc voltage on the breakdown performance of SF_6

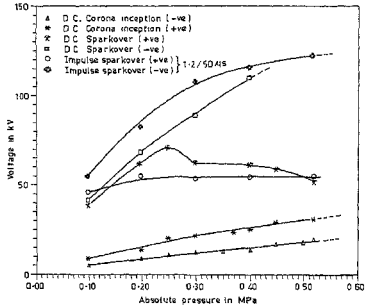

FIG. 2. Sparkover and corona inception voltage of SF_6 as a function of pressure for the needle-plane gap (needle dia = 0·54 mm, gap separation d = 10 mm).

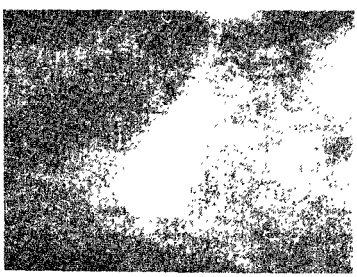

FIG. 4. Curved spark at 0·3 MPa; positive dc applied to needle.

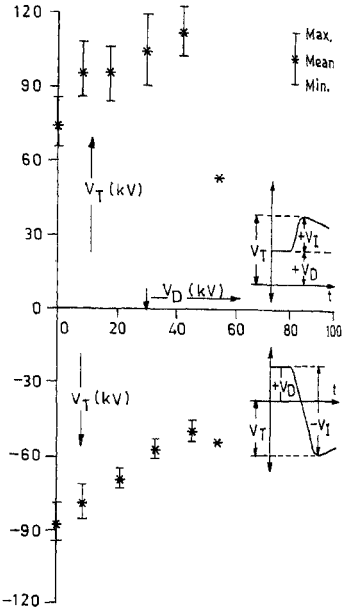

FIG. 3. Effect of dc bias on the total breakdown voltage in SF_6 at 0·2 MPa, for the rod-plane gap (rod dia = 2·17 mm; gap separation d = 10 mm)

2. LUXA, G., KYNAST, E. PIGINI, A., BARGIGIA, A., BOECK, W., HIESINGER, H SCHLICHT, S., WEIGART, N. AND ULLRICH, L

under impulse voltage, *Proc Inter. Symp. on Gaseous Dielectrics*, Knoxville. Tennessee, USA, March 1978.

Recent research activity on the dielectric performance of SF_6 with special reference to very fast transients, CIGRE 1988, 15–06.

3. WIEGART, N., NIEMEYER, L. PINNEKAMP, F., BOECK, W KINDERSBERGER, J., MARROW, M., ZAENGL, W., ZWICKY, W. GALLIMBERTI, I AND BOGGS, S. A.

Inhomogeneous field breakdown in GIS–The prediction of breakdown probabilities and voltages, Part I: Overview of a theory for inhomogeneous field breakdown in SF_6, *IEEE Trans*, 1988, **PD-3**, 923–930.

4. SANGKASAAD, S.

Dielectric strength of compressed SF_6 in nonuniform fields, Diss. ETH No 5738, ETH, Zurich, 1976.

5. ANIS, H. AND SRIVATSAVA, K. D

Non-uniform field breakdown of SF_6 insulation under combined ac and switching impulse voltages, *IEEE Trans.*, 1982, **PAS-101**, 3097–3104.

Thesis Abstract (M.Sc. (Engng))

Modulo–PCM codec implementation using single TMS 32010 digital signal processor by H. R. Ramanujam

Research supervisors: A. P. Shivaprasad and P. V. Ananda Mohan

Department: Electrical Communication Engineering

1. Introduction

The CCITT standardised algorithm for the ADPCM coder uses adaptive quantizer and adaptive predictors of order six with two poles and six zeros. It is quite cumbersome to implement the algorithm in VLSI form and requires the use of dedicated signal processors. The modulo-PCM (MPCM)[1] coding technique proposed by Ramamoorthy is simpler compared to the ADPCM. In this scheme, only the fractional part of the speech sample is coded and transmitted using 4 bits. This fractional part is computed based on a parameter 'd' which is computed for every block of 100 samples by choosing the absolute maximum of the adjacent sample differences within this block The parameter 'd' is also coded and transmitted as 'side information' at the rate of 800 bits per second along with the main speech data Thus, the gross bit rate becomes 32·8 kbs. At the receiver, the integer part is computed using 'd' and a first-order predictor. This integer part is then added to the decoded fractional part for the reconstruction of the speech sample.

2. Modulo-PCM codec

In view of the simplicity of the MPCM, its implementation using commercially available digital signal processors (DSP chips) has been attempted. For implementing this codec in stand-alone chip, TMS 32010[2] is found to be an ideal choice because it has the requisite number of on chip data RAM and programme ROM with the necessary processing power. Hence, the MPCM codec was built using the TMS 32010 analog interface board in conjuction with the evaluation module. The analog interface board has analog-to-digital converters and digital-to-analog converters with 12-bit resolution. It also has anti-aliasing and smoothing filters. The MPCM was tested for its speech quality and it was found to be satisfactory. Then, various CCITT-specified tests for speech, namely, linearity, frequency response, quantization distortion and idle channel noise were carried out using a standard PCM tester. Also, before implementing the MPCM codec on TMS 32010, its algorithm was verified by simulating the codec in FORTRAN on VAX-11 computer and results on SNR at different frequencies and input signal levels were obtained.

3. Conclusions

Both the software and the hardware aspects of the Modulo-PCM are considered and the results of the simulation as well as the hardware tests conducted using the analog interface board are presented. These results have confirmed the feasibility of an economical implementation of the MPCM coder for speech signal using the DSP chip.

References

1. RAMAMOORTHY, V. A novel speech coder for medium and high bit rate applications using Modulo-PCM principle, *IEEE Trans.*, 1985, **ASSP-33**, 356–368.

2. 32 kb/s ADPCM with the TMS 32010, Application Notes, Texas Instruments, 1985, pp. 469–497.

Thesis Abstract (M.Sc. (Engng))

Investigations of total pressure distortion of an aircraft intake model by T. K. Lokabhiram

Research supervisors: S. P. Govindaraju and M. S. Narayana (HAL)

Department: Aerospace Engineering

1. Introduction

Total pressure distortion generated by the intake of a fighter-type aircraft imposes serious limitations on

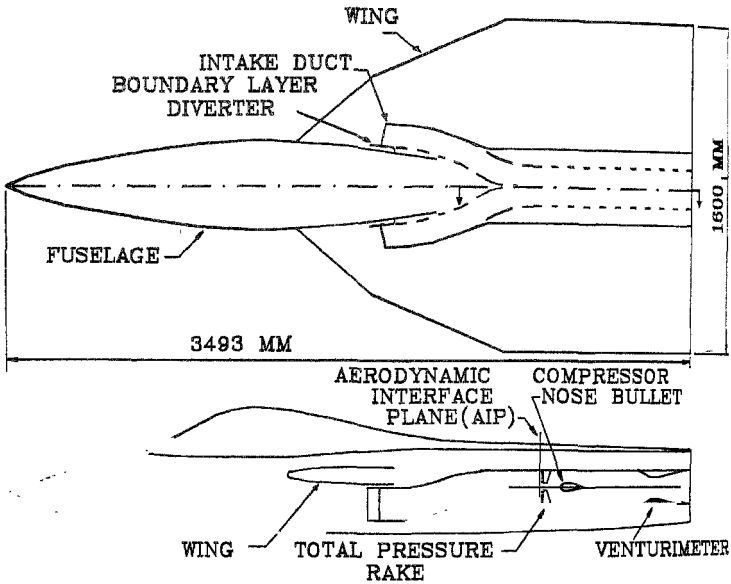

FIG. 1. Details of intake model.

the operation of its engine[1]. The experimental study and the follow up analysis reported here were conducted on an air intake model corresponding to a fighter aircraft configuration (Fig.1). The instrumentation of the aerodynamic interface plane (AIP) for measuring the steady state and fluctuating pressure signals and computer-based data acquisition systems were developed by the author who also developed the software for data acquisition and analysis.

Measurement of distortion is usually undertaken to evaluate the intake/engine compatibility during the development of an aircraft[2]. There can be instances when the evaluation of distortion levels in already existing intake configurations is required, like in prototype testing and pilot training. In such cases, it is possible to reduce flight test instrumentation required if a knowledge of the behaviour of the intake is available from model tests. With this possibility, the test data have been analysed and reviewed and it is shown that the distortion levels can be evaluated accurately using data from a limited number of total pressure probes. The same knowledge is also useful in selecting appropriate estimation technique for monitoring distortion and forecasting maximum distortion levels, with minimal instrumentation.

2. Test setup and instrumentation

The tests were conducted on a 1/3rd scale model of a futuristic fighter aircraft in the 14' × 9' Open Circuit Wind Tunnel at IISc. New instrumentation systems were developed to meet the specific needs of intake testing. The AIP was instrumented with 8 total pressure rakes, each having 5 total pressure probes. An ejector was used for simulating the engine mass flow through the intake. The 40 total pressure probes

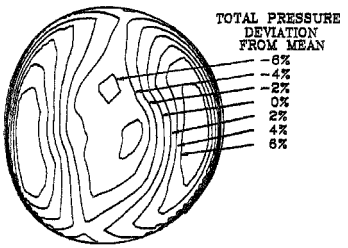

FIG. 2. Typical total pressure contours at AIP

contained in 8 rakes at the AIP were connected to two scannivalves mounted inside the mode. A pressure data acquisition system based on a PC/AT microcomputer was specially developed and used for these tests. Steady-state distortion evaluation had been done with the model attitude of $\alpha = 0$ to 30° and $\psi = 0$ and 5° and free stream velocity of 33 and 45 m/s.

High-frequency response Kulite transducers of 0.093″ diameter and a high-speed data acquisition system were configured for the measurement of fluctuating pressures at the AIP. A limited number of tests were carried out with the model attitude of $\alpha = 0$ to 30°, $\psi = 0$ and 5°. Several computer programs have been developed to edit, validate and process the pressure data for obtaining pressure recovery, distortion descriptors and contour maps. Figure 2 shows a typical pressure contour map. The distortion calculation was based on GE's (General Electric Company, USA) methodology. Statistical analysis was also carried out to find the character of the fluctuating pressures.

3. Analysis of data

The total pressure recovery is defined as

Total pressure recovery = $(\Sigma P_i/40) / P_f \times 100\%$

where P_i = total pressure at probe,

P_f = free stream total pressure.

The total pressure recovery is found to be good (88 to 92 %) for all the cases tested. The recovery increases with α up to 20° and this can be attributed to wing sheilding. Instantaneous recovery has shown higher values.

For the same ejector conditions, there is a reduction of mass flow in the intake of about 0·4 kg/s (7%) when α is increased form 0 to 30°. Dynamic tests also show a similar reduction in the mass flow.

The maps of steady-state total pressure across AIP have shown that there are two distinct crescent-shaped high-pressure zones due to flows from the two legs of the bifurcated duct. The flow pattern remains symmetrical up to $\alpha = 20°$ about plane of symmety of the model. Maps of instantaneous total pressure show random pattern due to pressure fluctuations.

GE distortion descriptors IDC and IDR are calculated using the following definitions.

Maximum circumferential distortion IDC is given by

Maximum IDC = Max. of [(IDC1 + IDC2)/2 . . . (IDC4 + IDC5)/2]

where IDC1. . .IDC5 are circumferential distortion on each ring given by

$$\text{IDC} = \frac{P_{AVG,i} - P_{MIN,i}}{P_{AVG}} \times EX(\theta_i) \qquad i = 1 \text{ to } 5 \text{ rings}$$

The radial distortion IDR is given by

$$\text{IDR} = \frac{P_{AVG} - P_{AVG,i}}{P_{AVG}} \qquad i = 1 \text{ to } 5 \text{ rings.}$$

$P_{AVG,i}$ is average pressure on ring i, $P_{Min,i}$ the minimum pressure on ring i, P_{AVG}, the face average pressure, and EX (θ_i), the extent factor

With α varying from 0 to 30°, the steady-state IDC is approximately constant and IDR has shown a decreasing trend. Maximum dynamic distortions have increased with α. The occurrence of distortion with values between 90 and 100% of their maximum value is randomly distributed during the test.

Analysis of steady-state test data and dynamic test data has shown that the low-pressure areas that contribute to distortion lie around probes situated in the centre portion of AIP for this intake. Hence, measurement of total pressure at these locations is sufficient for distortion evaluation. Reduced number of probes at AIP means less instrumentation requirements for flight testing the intake configuration.

Fluctuating pressure signals are checked for stationarity, power spectrum and amplitude distribution. The mean and RMS values are constant within 9%. Power spectrum obtained from the data showed approximately flat frequency response in most cases and the amplitude probability density function has normal distribution. Knowing the character of pressure fluctuations the distortion values can be monitored on line using a prediction technique and when implemented with other engine operating parameters, can serve as a surge warning to the pilot in prototype testing.

4. Conclusions

As part of the work, support systems for undertaking intake tests have been developed for the IISc low-speed wind tunnel. Instrumentation for the evaluation of steady state and dynamic distortion has been successfully developed and validated. Development and consolidation of many computer programs has been achieved. This will also meet any data processing needs for future intake tests.

The total pressure recovery of the intake model which was tested is found to be good. Mass-flow variation is about 7% with variation of α. While the steady-state total pressure contours show reasonable symmetry, instantaneous pressure contours show random patterns. Maximum values of distortions occurred with $\alpha = 30°$ and $\psi = 5°$. The random occurrence of IDC and IDR with values between 90 and 100% of their maximum values is useful in forecasting a probable peak distortion condition. As the low-pressure zones were found to lie at the centre of the AIP, pressure measurements in this area are sufficient to evaluate distortion accurately for the model tested. Use of such limited measurements for estimating distortion leads to significant savings in instrumentation and simplification in flight test procedures. In this context, normal distribution and flat power spectra are highly desirable characteristics. The distortion values evaluated with limited number of probes is accurate and comparable to that of 40 probe arrangement recommended by the engine manufacturer.

References

1. *Distortion-induced engine instability*, AGARD LS-72, 1972.
2. *Inlet total pressure distortion considerations for gas turbine engines*, Aerospace Information Report AIR 1419, SAE Aerospace Council Division, May 1973.

Thesis Abstract (Ph.D.)

Wing body configurations with segmented flaps by B.Rajeswari
Research supervisors: V. S. Holla, H. N. V. Dutt (NAL) and M. Shivakumaraswamy (NAL)
Department: Aerospace Engineering

1. Introduction

Flaps have been in use for a long time as devices to increase the lifting ability of wings, particularly to

improve low-speed performances, *viz.*, take-off and landing. In recent times, flaps have also been used to improve airplane performance at high speeds and in particular at high lift conditions encountered by high-performance airplanes during manoeuvres. Especially, spanwise segmented flaps both at leading and trailing edges are gaining increased use to generate optimum spanwise loading and to avoid tip stalling. With the emerging trend in aircraft design, wherein the computational tools are used right from the initial design phase, it is of immense importance to develop fast and reliable methods for the analysis of complex wings with deployed flaps.

2. Background and motivation for the current work

Even though several methods are available for the analysis of wing–body configurations based on both vortex lattice panel methods and singularity distribution panel methods, like, for example, methods of Margason and Lamar[1] & Woodward[2], the problem of wings with spanwise segmented flaps has not been considered in these methods. Wings with flaps can be analysed only in an indirect way by treating the flap portions as having additional incidence equal to flap deflection angle over and above that of free stream by these methods. Some of the methods like that of Dillenius *et al*[3] which can analyse wings with flaps are meant for some special-type flaps like jet-blown flaps.

Another very important aspect to be considered a priori in any program for the analysis of complex geometries, which has been hitherto neglected greatly in literature, is the development of highly versatile geometric input procedures. This is specially more critical for analysis of wings with flaps using vortex lattice methods wherein a stable numerical result depends to a large degree on geometric layout of lattice.

With this in view, in the present investigation, very efficient numerical methods within the philosophy of simple vortex lattice and source panel techniques have been developed for the analysis of wing–body–flap configurations in compressible inviscid flows. The emphasis of the work is on the analysis of spanwise segmented flaps both at leading and trailing edges. The most important task is to develop a model for flow near wing-flap gaps and program the procedures in a highly optimum way for computer core and time so that these can be run on small computing systems including personal computers.

3. Summary of the present work

3.1 *Analysis of simple wings with spanwise segmented flaps by planar horse shoe vortex lattice method*

One of the very widely used methods in thin-wing theory is the planar horse shoe vortex lattice method which is well developed and documented in literature for plane wings. This method has been extended to the problem of analysis of simple swept-tampered wings with spanwise segmented flaps at leading and trailing edges. Extensive numerical experimentations have been carried out to establish the criterion for rapid convergence of the numerical solution, especially as applied to wings with flaps. Also the problems near wing-flap junctures have been studied in detail and the remedial measures adopted numerically to overcome these problems suggested. Another important aspect considered here is the development of appropriate method of applying compressibility corrections, especially for flap configurations.

3.2 *Non-planar vortex lattice method for arbitrary wing–flap configurations*

In the planar horse shoe vortex lattice method, the trailing legs leave the wing surface in the plane of the panel to infinity. Since it is physically appropriate to graze the trailing vortices on the wing surface up to trailing edge and then make trail to infinity, a non-planar vortex lattice method has been developed to analyse wing–flap configurations. This program can analyse wings with complex geometries with deflected flaps and can treat an additional lifting surface. A very important, hitherto unaddressed problem of modelling of flow near wing–flap juncture, has been dealt with in detail. The effect of flap gap modelling has been clearly demonstrated by applying it to typical configurations of increasing complexity. Very large computing time reduction has been achieved by high level of optimisation used in programming the method. The results of a typical wing–flap case with flap deflected by 10°, with and without gap modelling, is presented in Fig. 1 from which the improvement in the results with gap modelling predicting the correct behaviour of c_p values near wing–flap juncture can be observed.

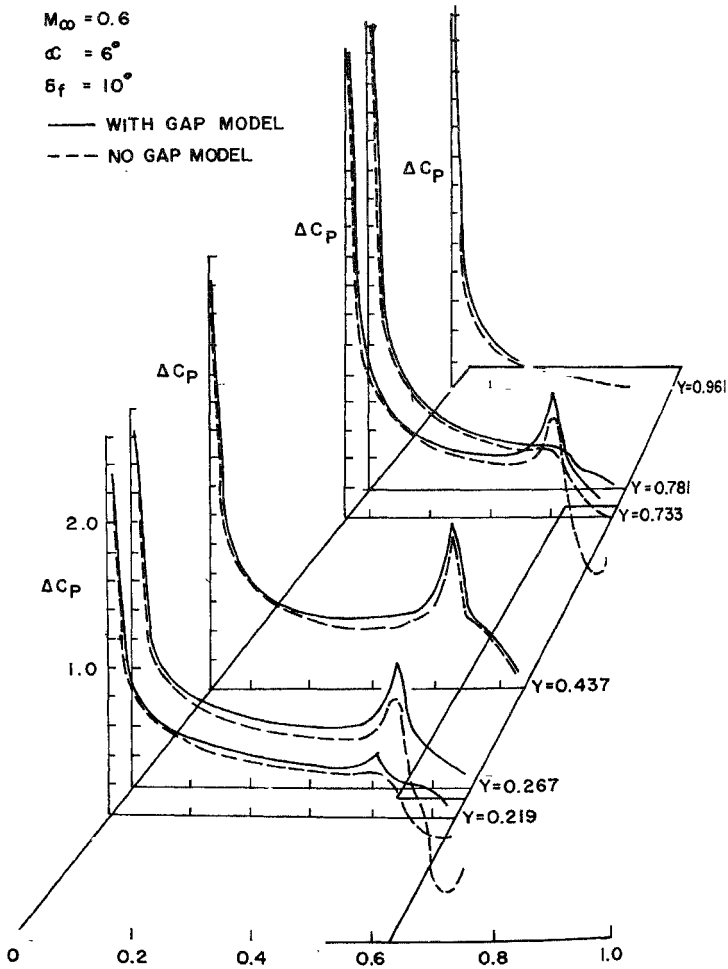

FIG. 1. ΔC_p distribution at various spanwise stations.

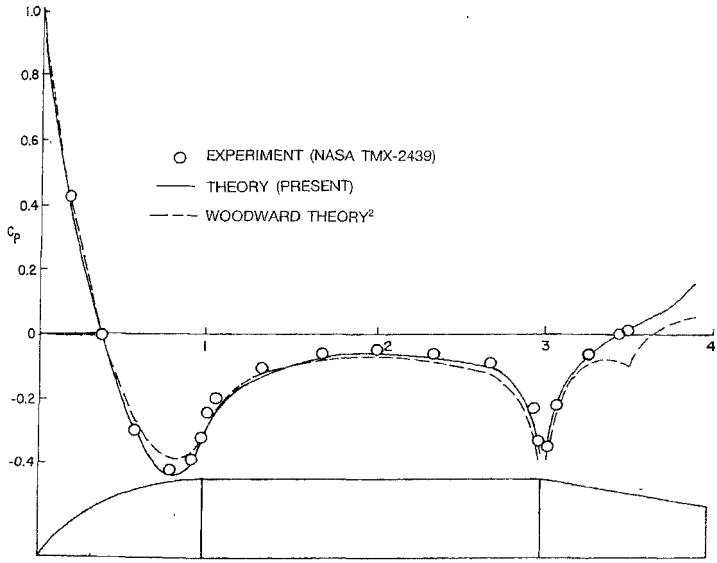

FIG. 2. C_p distribution on a tangent–ogive–boat tail body: comparison with experimental and Woodward results.

3.3 *Wing thickness effects*

Using the principle of linear superposition to get the final solution, wing volume effects are included using a constant source flat panel method for estimating induced velocities created by wing thickness surface at zero incidence. The method used to estimate the wing thickness source strengths is devoid of any numerical difficulties near leading edge, as compared to a number of available methods based on the camber-thickness separation.

3.4 *Body effects*

As a logical conclusion to the analysis of wing-flap configuration, the effects of body are considered. Even though the well-known source panel method is used a combined analytical technique and an optimum way of programming to analyse arbitrary bodies has shown a computer time reduction by a factor of 6 to 8, thus increasing its utility on small computers. Typical result for a tangent–ogive–boat tail body is shown in Fig. 2 along with the results of Woodward[2]. As can be seen, the results of current work compare better with the experimental results than those of Woodward.

3.5. *Wing–body interference*

Different models have been tried out for wing–body interference problem to arrive at a model which gives C_p distribution comparable to experiments in wing–body interference region. Results obtained for a wing–body–flap configuration are shown in Fig. 3. As can be seen from the figure, there is good agreement between theory and experiment.

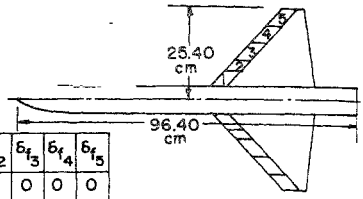

EXPT. (NASA TP 1351)	THEORY (Present)	δ_{f_1}	δ_{f_2}	δ_{f_3}	δ_{f_4}	δ_{f_5}
△	———	0	0	0	0	0
□	— — — —	4	4	4	8	8
○	— · — · —	0	8	12	16	20

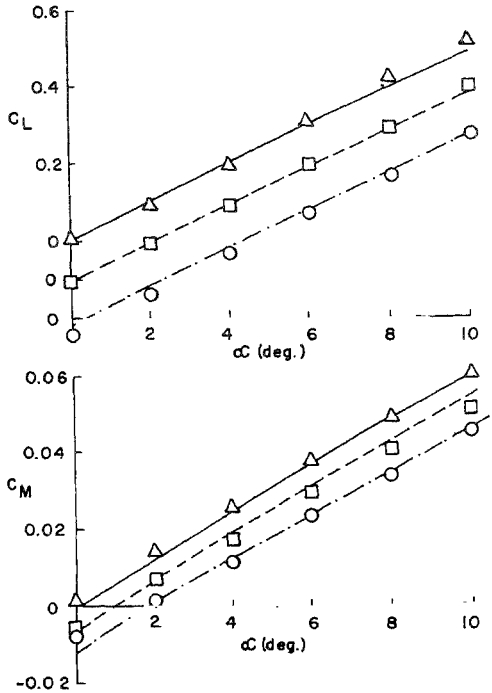

FIG 3. C_L *vs* α and C_M *vs* α curves for a wing–body–flap configuration.

4. Conclusions

Methods and computer programs have been developed to analyse arbitrary wing–body–flap configurations using the classical vortex lattice and constant source panel methods. Enough intelligence and logic have been built into the geometry package to automatically panel complex wing planforms with spanwise segmented flaps at both leading and trailing edges to generate lattice layout for producing numerically stable results with minimal input specifications. Improvements and optimisation in programming techniques have resulted in saving substantial amount of CPU time. New method to model the flow in the wing–flap juncture has been developed. A good comparison between theoretical and experimental values has been obtained, within the limits of linear inviscid theory, in δC_p, C_p and total forces and moments for various wing–tap configurations proving conclusively the validity of the techniques employed and methods developed in the current work.

References

1. MARGASON, R. J. AND LAMAR, J. E. — *Vortex lattice Fortran program for estimating subsonic aerodynamic characteristics of complex planforms*, NASA TN D-6142, 1971
2. WOODWARD, F. A. — *An improved method for the aerodynamic analysis of wing–body–tail configurations in subsonic and supersonic flow*, Parts I and II, NASA, CR–2228, 1973.
3. DILLENIUS, M. F. E., MENDENHALL, M. R. AND SPANGLER, S. B — *Calculation of longitudinal aerodynamic characteristics of STOL A/C with externally blown jet augmented flaps*, NASA CR–2358, 1974

Thesis Abstract (M.Sc. (Engng))

A comparative study and assessment of human resource development practices as perceived by scientists and engineers by P. K. Subramanya Swamy

Research supervisors: K.B. Akhilesh and A. A. Natarajan (NGEF)
Department: Management Studies

1. Introduction

The contribution of science and technology to social and economic well being of a nation was aptly recognised by the Indian Science Policy Resolution 1958. This has resulted in considerable investment in research and development activities. Several measures like tax benefits, import facilities, etc., were extended to encourage research in industries. Though the growth in science and technology is quite impressive, contributions of R&D are subjected to severe criticism[1]. Scientists and engineers constitute the core of human resources and are considered as a leverage to achieve organizational excellence[2,3]. Studies on R&D management have indicated that the performance of scientists and engineers is a complex phenomena influenced by several factors[4].

2. Objectives

The main purpose of the present study was to explore and describe the current human resource development practices with respect to the performance and satisfaction of scientists and engineers. The major objectives of the study were:

(i) to define and measure human resource development dimensions as perceived by R&D personnel.
(ii) to compare human resource development dimensions among R&D groups of manufacturing organizations.
(iii) to critically evaluate human resource development practices in relation to moderator (organizational climate, organizational structure, technology) and output variables (job satisfaction, performance, job involvement, obsolescence, reward satisfaction and career satisfaction).
(iv) to suggest appropriate actions for effective human resource development of Indian R&D personnel.

. Methodology

nitially, a theoretical research model was proposed, which served as a basis to consider the variables to e included, to define the variables, to decide the method of data collection and analysis. Based on the efinition of variables, a 75-item questionnaire was developed, standardised and used to collect the data.

Three R&D divisions, one each from the state public sector, central public sector and private sector /ere chosen for the study. One hundred and forty scientists and engineers of these organisations partici- ated in the study.

The data were analysed in two phases. Initially, the respondents were grouped according to their age nd qualifications. The difference in the perception of the variables was tested for their significance. Later, he same analogy was extended to compare the human resource development dimensions across the organi- ations. In the second phase of data analysis a normal correlation model was used to relate the human esource development dimensions with human resource development outcomes and the moderator vari- bles.

. Results and discussion

)ata analysis of the state public sector indicated that human resource development dimensions were rated rom average to somewhat above average. There was no significant difference in the perception of the ariables among different groups of respondents. Several human resource development dimensions were ated high among others. These include greater focus on utilization of capabilities while planning for ianpower, increased organizational involvement in recruitment and selection, greater role clarity during nduction, assignment of critical tasks while designing jobs, scope for utilization of appraisal feedback, and he indication of need for self-development.

Correlation analysis indicated strong linkages between the resource development dimensions and the uman resource development outcomes, namely, job satisfaction and job involvement. Job design seems o be the only human resource development dimension influencing the performance of the scientists and ngineers. Moderator variables, organizational climate and technology had significant relations with human esource development dimensions, whereas the moderator variable, organizational structure, did not indi- ate significant linkages.

Data analysis of the central public sector has indicated that the effectiveness of the human resource levelopment dimensions was perceived somewhat lower than average. The elders perceived the job design nd induction practices better than youngsters; similarly, graduates perceived better induction practices han post-graduates. Flexibility of manpower planning in assigning suitable tasks in the case of termination of R&D projects, organizational involvement in recruitment and selection practices, providing role clarity luring induction, assigning critical tasks while designing jobs, satisfaction over the utilization of appraisal eedback and the need to develop skills were rated higher among the variables.

Correlation analysis indicated that all the human resource development dimensions had significant rela- ions with job satisfaction, performance and career satisfaction. The moderator variables, organizational limate and technology, had strong linkages with human resource development dimensions, whereas the rganizational structure did not show any significant relationship.

Data analysis of the private sector has shown that all the human resource development dimensions were ated above average. There was no significant difference in the perception of the human resource develop- nent dimensions among the different groups of scientists and engineers. Flexibility in assigning alternative asks in the case of termination of projects, organizational involvement in recruitment and selection, pro- iding role clarity during induction, variety and autonomy while designing jobs, utilization of appraisal eedback for salary administration and for reward, the need for self development were rated high among he variables. Job satisfaction was the only human resource development outcome that had significant elationship with all the human resource development dimensions. Micro climate had strong linkage with ll the human resource development dimensions while organizational structure did not indicate any signific- nt relationship.

A comparison of human resource development dimensions across the organizations indicated that scientists and engineers of the private sector had better perception than their counterparts in the public sector. Among the public sector units, research personnel of the state public sector had better perception. Analysis indicated that scientists and engineers who had perceived the human resource development dimensions high have also perceived the human resource development outcomes as high and *vice versa*.

5. Conclusion

The present study has developed measures for assessing the effectiveness of human resource development practices. It has helped to understand the perception of human resource development dimensions by different groups of scientists and engineers. The study has revealed significant relationships between the human resource development dimensions and the human resource development outcomes as well as the moderator variables.

References

1. QUAZI, M. — What ails Indian science?, *Econ. Times*, April 1, 1987.

2. JAUCH, L. R., GLUECK, W F. AND OSBORN, R. M — Organizational loyalty, professional commitment and academic research productivity, *Acad. Res. Mgmt J.*, 1978, **21**, 84–92.

3 BADAWY, M K. — Managing human resources, *Res. Mgmt*, Sept–Oct 1988, 19–35.

4. DALTON, G. W. AND THOMPSON, P.H. — *Strategies for career management*, 1986, pp. 7–12, Scott Foresman.